Transport parameters for sound propagation in air saturated motionless porous materials: A review

Elio Di Giulio, Camille Perrot, Raffaele Dragonetti

International Journal of Heat and Fluid Flow 108 (2024) 109426

Contents lists available at ScienceDirect

International Journal of Heat and Fluid Flow

journal homepage: www.elsevier.com/locate/ijhff

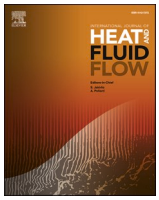

Transport parameters for sound propagation in air saturated motionless porous materials: A review

Elio Di Giulio [a,*,1], Camille Perrot [b], Raffaele Dragonetti [a]

[a] Department of Industrial Engineering, University of Naples Federico II, 80125 Naples, Italy
[b] Univ Gustave Eiffel, Univ Paris Est Creteil, CNRS, UMR 8208, MSME, F-77454 Marne-la-Vallée, France

ARTICLE INFO

Keywords:
Transport parameters
Sound absorption
Permeability
Characteristic length
Tortuosity

ABSTRACT

Transport parameters play a key role in characterizing the thermo-viscous behaviour of the microgeometry. Semi-phenomenological models provide valuable tools to establish a connection between the dynamic behaviour of porous materials and these transport parameters. However, each model has its limitations in terms of the frequency range and material types it can accurately represent. One of the most used semi-phenomenological acoustic models in the literature is the Johnson-Champoux-Allard-Lafarge (JCAL) model [J. Fluid. Mech. 176 (1987) 379–402, J. App. Phy. 70 (1998) 1975, J. Ac. Soc. Am. 102 (1998) 1995]. This model requires the knowledge of six transport parameters, known as the porosity φ, airflow resistivity σ, thermal characteristic length Λ', viscous characteristic length Λ, high-frequency limit of tortuosity α_∞, and static thermal permeability k_0', which establish a connection between the micro-geometrical features of the porous material and its macroscopic behaviour when subjected to sound waves. The JCAL model is applicable to all types of porous materials, and the required transport parameters can be measured using suitable devices. With recent advancements in additive manufacturing, it is now possible to create porous materials with precise and controlled geometries. Therefore, understanding the relationships between microgeometry and transport parameters is crucial for designing porous materials with specific acoustic properties. This study provides a comprehensive overview of all the transport parameters involved in characterizing the JCAL model. It synthesizes various direct, indirect, and inverse measurement techniques used to assess these parameters. Additionally, computational approaches for evaluating the transport parameters from representative elementary volumes (REV) of materials are presented. Finally, the study compiles the existing correlations between transport parameters and the microgeometry of the unit cell from the available literature.

1. Introduction

Porous materials are generally employed in different acoustic application (Allard and Atalla, 2009; Swift, 1998). Sound wave propagation in air fulfilling porous media can be described solving Navier-Stokes equations, coupled with continuity and energy equations. If the stiffness, or the weight, of material is much greater than the one of fluid, the frame of material can be considered rigid and motionless (Zwikker et al., 1949). Following the homogenization theory, when the wavelength is much greater than the medium pore size of the porous media, the description of viscous and thermal effects can be separated (Allard and Atalla, 2009). In acoustics, Zwikker and Kosten (Zwikker et al., 1949) introduces complex quantities, such as density $\widetilde{\rho}$ and bulk modulus $\widetilde{K}$, to describe the behaviour of porous material as an equivalent fluid. In thermoacoustics, Rott (Rott, 1969) (and then Swift (Swift, 1998) defined thermoviscous function f_ν and f_κ to characterize the viscous-thermal interaction between the solid skeleton and the oscillating fluid. From a fluid-dynamic point of view, the dynamic behaviour of a fluid flow fulfilling a porous core can be expressed in terms of complex Friction Factor f and Nusselt number Nu (Lu and Cheng, 2012). It can be demonstrated that all approaches are equivalent to characterize the thermoviscous behaviour of the material. In fact, Dragonetti et al. (Dragonetti et al., 2016) pointed out the equivalence between acoustic and thermoacoustic description of porous materials. Biot (Biot, 1956; Biot, 2005) defined a complex correction factor for the viscosity in dynamic regime. Lu and Garret (Liu and Garrett, 2006) explicates the

* Corresponding author.
E-mail address: elio.digiulio@unina.it (E. Di Giulio).
[1] ORCID: 0000-0003-0218-9719.

https://doi.org/10.1016/j.ijheatfluidflow.2024.109426
Received 13 November 2023; Received in revised form 10 May 2024; Accepted 10 May 2024
Available online 3 June 2024

relation between complex Nusselt number and thermal function f_κ. Di Meglio et al. (Di Meglio et al., 2022) underlined the possibility to characterize macroscopically a porous material under oscillating flow condition through a complex Darcy number and a complex Nusselt number to describe the viscous and thermal dynamic behaviour, respectively.

Therefore, the complete thermoviscous characterization of a porous medium requires the knowledge of two dynamic frequency-depending parameters (i.e. the thermoviscous functions, or the dynamic friction factor and Nusselt number, or the complex density and complex bulk modulus, or the dynamic viscous and thermal tortuosity, dynamic viscous and thermal permeability).

In acoustics, different models have been developed to describe sound propagation in porous media. For simple uniform cross-section, such as circular pore, parallel slit, pin array, analytical solutions are available in literature depending only on geometrical parameters (Zwikker et al., 1949; Stinson, 1991). For random porous media, such as high porosity fibers, empirical correlations are provided by Delany and Bezley (Delany and Bazley, 1970), further revisited by Miki (Miki, 1990), where the airflow resistivity σ is required as input parameter. Said f the sound frequency, this empirical model can be considered reliable in the range $0.01 < f/\sigma < 1$, elsewhere it returns non-physical results. Wilson (Wilson, 1998) defined a middle frequency range model through the definition of the vorticity-mode relaxation time, and the entropy-mode relaxation time. This model does not fit the asymptotic behaviour in the low and high frequency range.

Semi-phenomenological models have been developed to characterize the behaviour of a general porous structure through the knowledge of static parameters, so-called *transport parameters*. In literature, two of the most widely used semi-phenomenological models are the Johnson-Champoux-Allard and the Johnson-Champoux-Allard-Lafarge model (Johnson et al., 1987; Champoux and Allard, 1998; Lafarge et al., 1998) (respectively JCA and JCAL for brevity). The first one requires the knowledge of five transport parameters: the porosity φ, the airflow resistivity σ, the thermal Λ' and viscous Λ characteristic lengths, the high frequency limit of tortuosity α_∞. In the JCAL model the static thermal permeability k_0' is introduced as new parameter to improve the description of the thermal effects. These all parameters link the microstructural features of the porous medium with its macroscopic behaviour. They are strictly linked with the high and low frequency asymptotic behaviour of the material. Furthermore, Pride *et al.* (Pride et al., 1993) introduced other two parameters, the static thermal α_0' and viscous α_0 tortuosity, to improve the low frequency description in case of pores with possible constriction (so-called JCAPL model). The frequency validity range of the JCAL model and the possibility of evaluating all the transport parameters numerically and experimentally make it the model largely in literature. The complete model (JCALP) is not diffused due to the impossibility to measure experimentally and to verify Pride's parameters values. They can be only evaluated numerically, once the micro-geometry is precisely known.

Recent developments in additive manufacturing made this technology suitable to realize porous materials with a controlled geometry process (Auriemma and Holovenko, 2019; di Giulio et al., 2021; Auriemma et al., 2020; Suárez and del Mar Espinosa, 2020). The goal of this study is to provide a review of transport parameters, specifically focusing on how they can be determined through numerical simulations when the microgeometry is known, and how they can be experimentally measured. Furthermore, the correlations of transport parameters found in the literature for various types of materials are reported. Once the required acoustic properties are fixed, the knowledge of these correlations represents a design tool able to characterize the geometry skeleton of the porous material. The outline of the paper is reported in follows. In Sec. 2, the Johnson-Champoux-Allard-Lafarge model is recalled with its asymptotic limit for complex density and bulk modulus and the definition of each transport parameters is given. Sec. 3 shows experimental technique to assess the transport parameters, while computational approaches are presented in Sec. 4. Subsequently, in Sec. 5 correlations for transport parameters from literature are collected and reported for different typology of unit cells, and materials.

2. Definitions of transport parameters

2.1. Johnson-Champoux-Allard-Lafarge model

The dynamic behaviour of porous material is described by the coupling between Linearized Navier Stokes, energy and continuity equations in frequency domain (said $\omega = 2\pi f$ the angular frequency)

$$i\omega\rho_0 v_1 = -\frac{dp_1}{dx} + \mu\nabla^2 v_1, \tag{1}$$

$$i\omega\rho_0 c_p T_1 = i\omega p_1 + k\nabla^2 T_1, \tag{2}$$

$$i\omega\rho_1 + \nabla\cdot(\rho_0 v_1) = 0. \tag{3}$$

In these equations, each thermodynamic quantity (p, ρ, T) is expressed as sum of a static term (subscript 0) and a harmonic one (subscript 1), while velocity has only a harmonic component as consequence of no static pressure gradient. $\mu, \kappa, \rho_0, c_p, \gamma$ are respectively the dynamic viscosity, the thermal conductivity, the medium density, the specific heat at constant pressure and the heat capacity ratio of the fluid. The time notation chosen agrees with $i\omega t$, where $i = \sqrt{-1}$. The existence of a microscopic characteristic length l, determined by the size of local heterogeneities or the period size of the material, and a macroscopic characteristic length $L = \lambda/2\pi$, where $\lambda = c/f$ is the sound wavelength with c the speed of sound, and their highly distinct values, i.e. $l/L \ll 1$, permit defining a Representative Elementary Volume, see Fig. 1 (Auriault et al., 2010). Therefore, under scale separation between the wavelength and the characteristic size of the pore (as highlighted by Kirchhoff (Kirchhoff, 1868) for $r_w^{3/2} f < 10^{-6}\text{cm}\cdot\text{s}^{-3/2}$, with r_w the pore size being greater than 10^{-3}cm), momentum and energy equations allow to describe the visco-inertial and heat diffusion effect separately, together with the hypotheses of rigid and isothermal walls of the

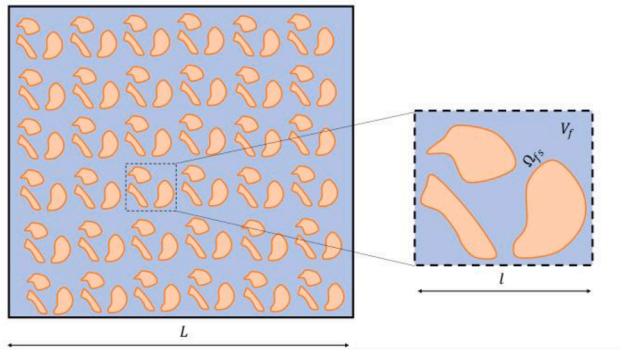

Fig. 1. On the left, macroscopic scale description, and on the right microscopic scale description of a periodic porous media.

material solid skeleton, Ω_{fs}: $v_1 = 0, T_1 = 0 \text{on} \Omega_{fs}$, general solutions of Eqs. (1), (2) can be written in terms of complex density and bulk modulus, following (Allard and Atalla, 2009):

$$\widetilde{\rho} = \frac{\rho_0}{F(\omega)}, \tag{4}$$

$$\widetilde{K} = \frac{\gamma p_0}{\gamma - (\gamma - 1)F(P_r\omega)}. \tag{5}$$

Here $P_r = \kappa/\mu c_p$ is the Prandtl number, and F is the function which describes viscous and thermal dissipations inside the porous material. F depends on the microgeometry of the material and the viscous and thermal boundary layer defined as $\delta_\nu = (2\mu/\omega\rho_0)^{1/2}$ and $\delta_\kappa = (2k/\omega\rho_0 c_p)^{1/2}$.

The semi-phenomenological Johnson-Champoux-Allard-Lafarge model provides a separated description of the dynamic viscous (Johnson et al., 1987) and thermal behaviour (Champoux and Allard, 1998; Lafarge et al., 1998) of a porous medium through respectively the complex density $\widetilde{\rho}(\omega)$ (equivalent to complex viscous permeability $\widetilde{k}(\omega)$ and complex viscous tortuosity $\widetilde{\alpha}(\omega)$) and the complex bulk modulus $\widetilde{K}(\omega)$ (or which is the same, complex thermal permeability $\widetilde{k}'(\omega)$ and complex thermal tortuosity $\widetilde{\alpha}'(\omega)$). For visco-inertial effects

$$\widetilde{\rho} = \frac{\rho_0\alpha_\infty}{\varphi}\left[1 - i\frac{\omega_\nu}{\omega}\widetilde{G}(\omega)\right], \tag{6}$$

$$\widetilde{G}(\omega) = \sqrt{1 + \frac{1}{2}iM\frac{\omega}{\omega_\nu}}, \tag{7}$$

where

$$(a)M = \frac{8k_0\alpha_\infty}{\varphi\Lambda^2}; (b)\omega_\nu = \frac{\mu\varphi}{\rho_0 k_0\alpha_\infty}. \tag{8}$$

For thermal effects

$$\widetilde{K} = \frac{\gamma p_0/\varphi}{\gamma - (\gamma - 1)\left[1 - i\frac{\omega_\kappa}{\omega}\widetilde{G}'(\omega)\right]^{-1}}, \tag{9}$$

$$\widetilde{G}'(\omega) = \sqrt{1 + \frac{1}{2}iM'\frac{\omega}{\omega_\kappa}}, \tag{10}$$

$$(a)M' = \frac{8k_0'}{\varphi\Lambda'^2}; (b)\omega_\kappa = \frac{\kappa\varphi}{\rho_0 c_p k_0'}. \tag{11}$$

$M, M', \omega_\nu, \omega_\kappa$ are respectively the viscous and thermal pore shape factor and viscous and thermal reduced frequency. They allow to express the complex density and bulk modulus through dimensionless parameters.

The equivalence between the dynamic viscous parameters can be expressed through the Darcy's law in dynamic regime and the definition of dynamic tortuosity as follow (Johnson et al., 1987)

$$(a)\widetilde{k}(\omega) = \frac{\delta_\nu^2}{2i}\frac{\rho_0}{\widetilde{\rho}}; (b)\widetilde{\alpha}(\omega) = \frac{\widetilde{\rho}}{\rho_0}; (c)\widetilde{k}(\omega) = \frac{\delta_\nu^2}{2i\widetilde{\alpha}(\omega)}. \tag{12}$$

At the same time, for the thermal characterization it results

$$(a)\widetilde{k}'(\omega) = \frac{\delta_\kappa^2}{2i}\frac{\gamma}{\gamma - 1}\left(1 - \frac{p_0}{\widetilde{K}}\right); (b)\widetilde{\alpha}'(\omega) = \frac{\gamma - 1}{\gamma\left(1 - \frac{p_0}{\widetilde{K}}\right)}; (c)\widetilde{k}'(\omega) = \frac{\delta_\kappa^2}{2i\widetilde{\alpha}'(\omega)}. \tag{13}$$

The thermal characterization moves from an isothermal (low frequency) to adiabatic (high frequency) behaviour, while viscous losses prevail on inertia effects on low frequency and vice versa in high frequency regime.

The high and low frequencies are related to the ratio between the average pore size $\bar{r}$ and the thermal and viscous boundary layers.

At low frequency limit, for $\bar{r}/\delta_{\nu(\kappa)} \to 0$, complex density at first order approximation can be written as

$$\widetilde{\rho} = \frac{\rho_0}{\varphi}\left[\frac{\varphi}{2i}\frac{\delta_\nu^2}{k_0} + \alpha_\infty\left(1 + \frac{2k_0\alpha_\infty}{\varphi\Lambda^2}\right)\right] = \frac{\rho_0\alpha_\infty}{\varphi}\left(-i\frac{\omega_\nu}{\omega} + 1 + \frac{M}{4}\right), \tag{14}$$

and bulk modulus

$$\widetilde{K} = \frac{\frac{\gamma p_0}{\varphi}}{\gamma - (\gamma - 1)\left(\frac{\varphi}{2i}\frac{\delta_\kappa^2}{k_0'} + 1 + \frac{2k_0'}{\varphi\Lambda'^2}\right)^{-1}} = \frac{\gamma p_0/\varphi}{\gamma - (\gamma - 1)\left(-i\frac{\omega_\kappa}{\omega} + 1 + \frac{M'}{4}\right)^{-1}}. \tag{15}$$

Therefore, by combining Eqs. (14) and (15) respectively with Eqs. (12.a) and (13.a), it results that:

$$(a)\widetilde{k}(\omega) = \frac{1}{\frac{1}{k_0} + \frac{2i\alpha_\infty}{\varphi\delta_\nu^2}\left(1 + \frac{2k_0\alpha_\infty}{\varphi\Lambda^2}\right)}; (b)\widetilde{k}'(\omega) = \frac{1}{\frac{1}{k_0'} + \frac{2i}{\varphi\delta_\kappa^2}\left(1 + \frac{2k_0'}{\varphi\Lambda'^2}\right)}. \tag{16}$$

At high frequency limit, for $\bar{r}/\delta_{\nu(\kappa)} \to \infty$, inertial effects prevail on viscous behaviour, and it follows that:

$$\widetilde{\rho} = \frac{\rho_0\alpha_\infty}{\varphi}\left[1 + (1 - i)\frac{\delta_\nu}{\Lambda}\right] == \frac{\rho_0\alpha_\infty}{\varphi}\left[1 + \frac{(1 - i)}{2}\sqrt{\frac{\omega_\nu}{\omega}M}\right], \tag{17}$$

$$\widetilde{K} = \frac{\frac{\gamma p_0}{\varphi}}{\gamma - (\gamma - 1)\left[1 - (1 - i)\frac{\delta_\kappa}{\Lambda'}\right]^{-1}} == \frac{\gamma p_0/\varphi}{\gamma - (\gamma - 1)\left[1 - \frac{(1-i)}{2}\sqrt{\frac{\omega_\kappa}{\omega}M'}\right]^{-1}}. \tag{18}$$

Furthermore, dynamic viscous and thermal tortuosity in high frequency approximations can be expressed from Eqs. (12.b) and (13.b) as

$$(a)\widetilde{\alpha}(\omega) = \alpha_\infty\left[1 + (1 - i)\frac{\delta_\nu}{\Lambda}\right]; (b)\widetilde{\alpha}'(\omega) = \left[1 - (1 - i)\frac{\delta_\kappa}{\Lambda'}\right] \tag{19}$$

As it can be seen from Eqs. (14), (15), (17) and (18) low and high frequency dynamic behaviour of porous material are described respectively from the permeabilities and the high frequency limit of tortuosity and the characteristic lengths.

M and M' can be useful to check the consistency of the values of the transport parameters. For classical porous materials for acoustic applications, M and M' should have orders of magnitude around 1 (i.e. they are equal to 1 for straight cylindrical pore). In Figs. 2 and 3,

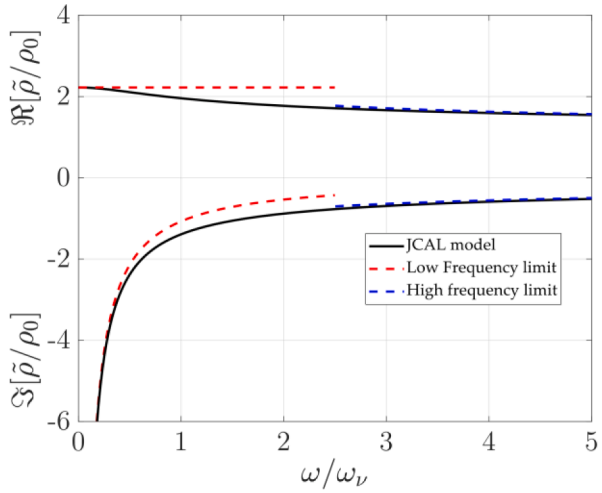

Fig. 2. Dimensionless complex density from JCAL model ($M = 4.3, \alpha_\infty = 1.05, \varphi = 0.98$).

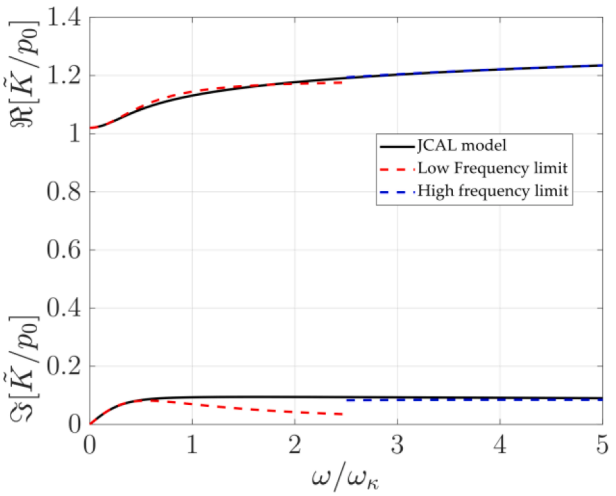

Fig. 3. Dimensionless complex bulk modulus from JCAL model ($M' = 4.3, \gamma = 1.4, \varphi = 0.98$).

dimensionless complex density $\widetilde{\rho}/\rho_0$ and bulk modulus $\widetilde{K}/p_0$ are reported respectively as function of the dimensionless set $(M, M', \alpha_\infty, \gamma, \varphi)$ versus dimensionless frequencies axis $\omega/\omega_\nu(\omega/\omega_\kappa)$, to be independent from fluid properties It is worth noticing that the Johnson model was developed for petroleum research and therefore concerns porous media saturated with liquids (water, oil, etc.) (Johnson et al., 1987). In these materials, only viscous effects are considered significant, as thermal effects are minimal in liquids carrying acoustic waves. On the other hand, if the fluid is a gas, Johnson's model requires significant modifications to include thermal effects and Biot parameters (Q and R) (Biot, 1956; Biot, 2005), which depend on the gas compressibility. The work by Allard, Champoux (Champoux and Allard, 1998), and Lafarge (Lafarge et al., 1998), which is derived from Johnson's model, introduces the *equivalent fluid* model, where acoustic waves propagate only within the pore space of the material, while the solid skeleton is considered motionless. Thus, the JCAL model is the model used for acoustic wave propagation in gas-saturated porous materials. Contributions from other researchers, such as Pride (Pride et al., 1993), though less directly relevant to users of the model, are nevertheless important for the theoretical advancement of the model.

2.1.1. Porosity

The porosity is defined as the relative fraction, by volume, of air contained within the material (Champoux et al., 1998), and it can be operatively written as the ratio between the fluid part volume V_f and the total volume of the material V_t

$$\varphi = \frac{V_f}{V_t} = \frac{V_f}{V_f + V_s} = 1 - \frac{\rho_b}{\rho_m}, \tag{20}$$

where V_s is the volume occupied by the solid skeleton. At the same time, porosity can be defined also considering the complement to unit of the ratio between the bulk density ρ_b of material and the density of the solid skeleton ρ_m.

2.1.2. Airflow resistivity

Airflow resistivity σ can be defined starting from the static viscous permeability (Perrot et al., 2008; Zhou and Sheng, 1989; Auriault et al., 1998). In turn, k_0 is defined as the low frequency limit of the dynamic viscous permeability $\widetilde{k}(\omega)$, Eq. (16.a). This latter parameter is defined in the dynamic Darcy's law in frequency domain:

$$\varphi\langle v\rangle = \frac{\widetilde{k}(\omega)}{\mu}\nabla p. \tag{21}$$

$\widetilde{k}(\omega)$ is defined as a second order symmetric depending on two vectorial quantities such as acoustic particle velocity $\langle v\rangle$ (square brackets indicates the volume average value) and the pressure gradient along a direction. k_0 is the reference value respect to the direction of wave propagations, and it is strictly related to σ from the relation

$$\sigma = \frac{\mu}{k_0}. \tag{22}$$

The airflow resistivity represents the most common parameters in the description of flow across porous media. Equivalently, it is also defined as the ratio between static pressure gradient and the fluid velocity across the material

$$\sigma = \frac{\Delta p}{d\langle v\rangle}, \tag{23}$$

where d is the sample thickness, Δp the pressure drops along the material and $\langle v\rangle$ is the average flow. Airflow resistivity unit is *Rayls* (equal to $Pa{\cdot}s/m^2$), while permeability has the dimension of an area m^2.

2.1.3. Thermal characteristic length

Thermal characteristic length is a geometrical quantity defined as twice the ratio between the volume of fluid V on the fluid–solid wet surface $\partial\Omega$ (Johnson et al., 1987)

$$\Lambda' = 2\frac{\int_{V_f} dV}{\int_{\partial\Omega} d\Omega}. \tag{24}$$

This parameter allows to describe the thermal exchange between fluid and solid skeleton due to the thermal effect generated by the compression and the rarefaction of particles. In particular, in the high frequency limit thermal effects can been seen only near the wall of the skeleton of the porous material.

2.1.4. Viscous characteristic length

Viscous characteristic length is defined in the high frequency limit where the effect of viscosity is overcome by the forces of inertia. Due to this fact, it is defined as twice the ratio of the weighted by the velocity in the volume to that of the surface of an inviscid (no viscosity) fluid (Johnson et al., 1987)

$$\Lambda = 2\frac{\int_{V_f} |v|^2 dV}{\int_{\partial\Omega} |v(\partial\Omega_{fs})|^2 d\Omega}, \tag{25}$$

where $\partial\Omega_{fs}$ represents the fluid–solid interface.

2.1.5. High frequency limit of tortuosity

The high frequency limit of tortuosity is an intrinsic dimensionless parameter which describes how tortuous is the path of a sound wave to propagate inside the porous material due to the irregularities of its solid skeleton. From a theoretical point of view, it can be obtained in the ideal case of inviscid fluid as (Allard and Atalla, 2009; Johnson et al., 1987):

$$\alpha_\infty = \frac{\frac{1}{V_f}\int_{V_f}|v^2|dV}{\left(\frac{1}{V_f}\int_{V_f}|v|dV\right)^2}. \tag{26}$$

When the effect of viscosity becomes negligible, at high frequency when the viscous penetration depth tends to zero, the effective fluid density tends to $\rho_0\alpha_\infty$.

2.1.6. Static thermal permeability

Lafarge *et al.* (Lafarge et al., 1998) introduced the dynamic thermal permeability $\widetilde{k}(\omega)$ to improve the description of low frequency thermal behaviour of porous media, by setting an analogous thermal Darcy's law similar to Eq. (21)

$$\varphi\langle T\rangle = \frac{\widetilde{k}(\omega)}{\kappa}\frac{\partial p}{\partial t}, \tag{27}$$

where $\langle T\rangle$ is the acoustic oscillating temperature averaged over the fluid volume. Analogously, static thermal permeability k_0' is defined as the low frequency limit of the thermal dynamic permeability, Eq. (16.b). The description of thermal behaviour involves scalar quantities such as the acoustic pressure and temperature fields. Therefore, thermal permeability is a scalar quantity depending only on the microgeometry of the material.

Torquato (Torquato, 1990) pointed out the relations between the permeability and the trapping constant Γ of porous media

$$k_0' = \frac{1}{\Gamma}. \tag{28}$$

In diffusion-controlled reactions problems, trapping constant is defined as

$$\Gamma = \frac{s}{\varphi\langle m\rangle D}, \tag{29}$$

where D and s are respectively the diffusion coefficient and the rate of production of reactant in a steady-state fluid region with volume V and $\partial\Omega$ the boundary surface between fluid and solid

$$D\nabla^2 m = -s, \#\text{in } V \tag{30}$$

$$m = 0.\#\text{on}\partial\Omega \tag{31}$$

3. Measurement techniques

Several metrological techniques have been developed to assess the transport parameters in porous materials, classified as direct, indirect, and inverse methods. Direct methods directly estimate a parameter, while the indirect method derives transport parameters from complex density and bulk modulus, using analytical formulations by Only and Panneton (Olny and Panneton, 2008; Panneton and Olny, 2006). Inverse methods employ optimization models to determine the transport parameter set those best fits experimental data.

3.1. Direct methods

Experimental techniques to evaluate each transport parameter are reported in the following. The methodologies found out in literature are collected in Table 1.

3.1.1. Porosity

In the literature different approaches are provided to assess the porosity of a porous material. Beranek (Beranek, 2005) proposed a method based on the height of the water in the two sides of the U manometer linked to a chamber containing the sample, Fig. 4.a. Leclaire *et al.* (Leclaire et al., 2003) showed a methodology based on the volume

Table 1
Transport parameters' direct measurement set up in literature.

Authors	Transport parameters	Method
Beranek (Beranek, 2005)	φ, σ	Volumes' method, Standard Test method
Leclaire et al. (Leclaire et al., (2003) 1366.)	φ	Comparison of air-volumes
Champoux et al. (Champoux et al., 1998)	φ	Air-based system
Salissou and Panneton (Salissou and Panneton, 2007)	φ	Pressure-mass method
Umnova et al. (Umnova et al., 2005)	φ, α_∞	Ultrasonic reflection and transmission measurements
Fellah et al. (Fellah et al., 2003)	φ, α_∞	Ultrasonic reflected waves at oblique incidence measurement
Fellah et al. (Fellah et al., 2002)	φ	Ultrasonic reflected waves measurement
Leonard (Leonard, 2005)	σ	Analytical balance method
ASTM C522 (American Society for Testing and Materials, 2017)	σ	Standard Test method
Bies and Hansen (Bies and Hansen, 1980)	σ	Standard set up
Brown and Bolt (Brown and Bolt, 2005)	σ	Standard set up
ISO 9053-1 (ISO - ISO 9053-1:2018, 2021)	σ	Standard Test method
Stinson (Stinson and Daigle, 1998)	σ	Electronic set up
ISO 9053-2 (ISO - ISO 9053-2:2020, 2021)	σ	Standard Alternating airflow method
Ingard and Dear (Ingard et al., 1985)	σ	Alternating airflow method
Dragonetti et al. (Dragonetti et al., 2011)	σ	Alternating airflow method
Smeulders et al. (Smeulders et al., 1992)	k_0	Alternating flow method
Charlaix et al. (Charlaix et al., 1988)	k_0	Alternating flow method
Leclaire et al. (Leclaire et al., 1998; Leclaire et al., 1998; Leclaire et al., 1998)	Λ, Λ'	Ultrasonic measurement set up
Fohr et al. (Fohr et al., n.d.)	Λ, α_∞	Double ultrasonic tests
Moussatov et al. (Moussatov et al., 2001)	Λ, α_∞	Ultrasonic measurement with static pressure variation
Ayrault et al. (Ayrault et al., 1999)	Λ, α_∞	Ultrasonic measurement with static pressure variation
Allard et al. (Allard et al., 1998)	α_∞	Ultrasonic measurement set up
Bonfiglio and Pompoli (Brown, 1980)	α_∞	Ultrasonic measurement set up
Henry and Allard (Debray et al., 1998)	k_0'	Measurement of low frequency limit of bulk modulus
Debray et al. (Tarnow, 1998)	k_0'	Measurement of low frequency limit of bulk modulus

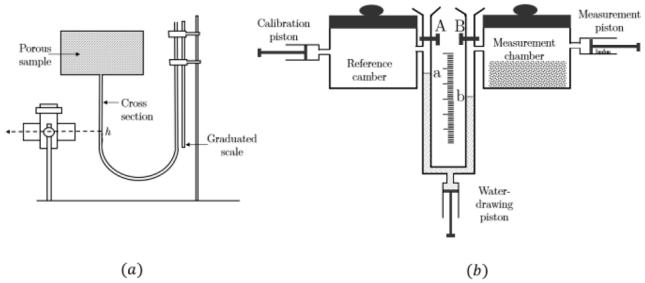

Fig. 4. Different porosity measurement systems: (a) Beranek's system (Beranek, 2005), (b) Comparison of air-volumes (Leclaire et al., 2003).

variation of the measurement chamber where the material is placed, due to a moving piston, as shown in Fig. 4.b. Champoux and Stinson (Champoux et al., 1998) evaluated the porosity though the use of a piston which produces a change in volume, and then a change in pressure which is measured with an electronic pressure transducer. Salissou and Panneton (Salissou and Panneton, 2007) provided a pressure/mass method based on four measurements in different operating conditions. Acoustical methodologies to assess the porosity value of a porous material are provided by Umnova *et al.* and Fellah (Umnova et al., 2005; Fellah et al., 2003; Fellah et al., 2002). In both works, porosity and tortuosity are determined. In these studies, the authors demonstrate measurement techniques utilizing the ultrasonic reflectivity method in a temporal model of both direct and inverse scattering problems. The reflection and transmission scattering operators are derived from the responses of the tested porous medium to an incident acoustic pulse at oblique incidence.

3.1.2. Airflow resistivity

This section presents different experimental methodologies to assess the airflow resistivity of porous materials (Tang and Yan, 2018). The methodologies are categorized into direct (or static) and alternating methods for better clarity. The first method is based on the definition of airflow resistivity, Eq. (23). It is based on the measuring the static pressure drops across the material sustaining a constant volume velocity (Leonard, 2005; American Society for Testing and Materials, 2017; Bies and Hansen, 1980; Brown and Bolt, 2005; ISO - ISO 9053-1:2018, 2021; Stinson and Daigle, 1998), as shown in Fig. 5. The ASTM C522 (American Society for Testing and Materials, 2017) provides a standard test method for airflow resistance of acoustical materials with $\sigma = 100\tilde{A}\cdot 10000 Rayls$. The test requires a suction generator, a flowmeter and differential pressure measuring device low linear velocity ($< 50 mm/s$) and low-pressure difference across the sample ($250 Pa$) are required to avoid turbulence and non-linear effect. Bies and Hansen (Bies and Hansen, 1980) also reproduced the set up reported in ASTM C522 and provided technical tips to take into account the typology of material (hard or soft skeleton) and to avoid air losses. Stinson (Stinson and Daigle, 1998) provides an electronic set up for the measurement both pressure drops and the mass flow rate as electric signals. This fact allows to reach the results 20–50 times faster than the mechanical devices and with a minor degree of uncertain.

Another method based on alternating airflow has also been standardized by ISO 9053-2 (ISO - ISO 9053-2:2020, 2021). This method requires an oscillating piston which generates an alternating flow across the sample at the frequency of 2 Hz, as it can be seen in Fig. 6.

Alternative acoustic method to evaluate airflow resistivity are presented by Ingard and Dear (Ingard et al., 1985) and Dragonetti *et al.* (Dragonetti et al., 2011). In the first one, the porous sample is inserted inside a cylindrical tube with a rigid termination and an acoustic source

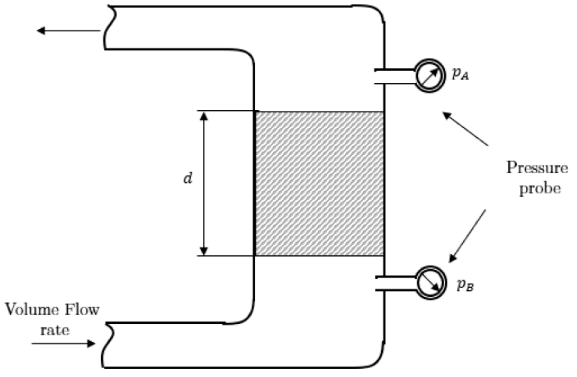

Fig. 5. Airflow resistivity measurement system: ISO 9053–1 Airflow resistivity measurement set up (ISO - ISO 9053-1:2018, 2021).

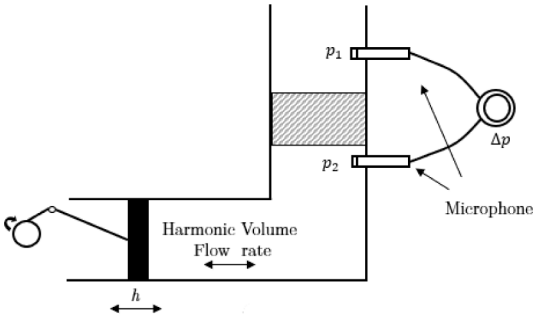

Fig. 6. Alternating airflow method for measuring airflow resistance, ISO 9053 (ISO - ISO 9053-2:2020, 2021).

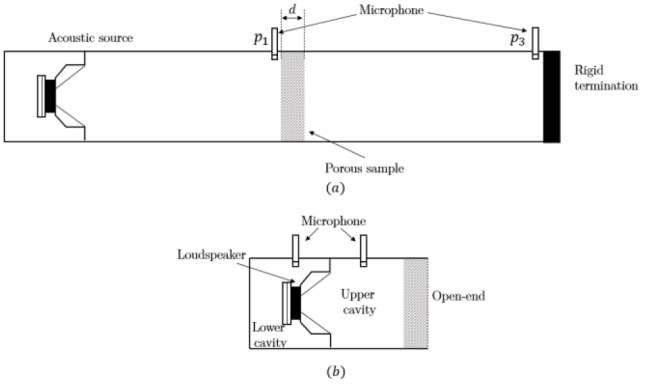

Fig. 7. Acoustic method to measure airflow resistivity: (a) (a) Dragonetti et al. set up (Dragonetti et al., 2011), (b) Ingard and Dear set up (Ingard et al., 1985).

in the other side, as shown in Fig. 7.a. By measuring the acoustic pressure in two different point, (Ingard et al., 1985) provided the formula to assess the airflow resistivity:

$$\sigma = \rho_0 c_0 \left| \Im\left(\frac{p_1}{p_2}\right) \right|, \tag{32}$$

where c_0 is the sound speed in free air, and $\Im$ indicates the imaginary part of a complex number. Dragonetti *at al.* (Dragonetti et al., 2011) showed the possibility to evaluate airflow resistivity though an equivalent electro-acoustic network, by measuring the acoustic pressures p_{up} inside the cavity (in which the sample is placed) and p_{dw} in the back cavity of the loudspeaker, see Fig. 7.b. From the p_{dw} measurement it is then possible to obtain the acoustic volume velocity which crosses the porous material. In a range where the imaginary part of the ratio between these two acoustic pressures is linear with the frequency, airflow resistivity can be estimated as

$$\sigma = \frac{\Im\left(\frac{p_{up}}{p_{dw}}\right)}{-\frac{\omega V_{dw}}{\gamma P_0 S} d}. \tag{33}$$

V_{dw} and S are respectively the air volume of the back cavity of the loudspeaker and the cross-sectional area of the tube where the sample is placed.

Experimental studies have also been carried out by analysing the dynamic permeability in porous media (Smeulders et al., 1992; Charlaix et al., 1988). Charlaix *et al.* (Charlaix et al., 1988) provided an oscillatory flow by means of an audio speaker driving a soft membrane (Fig. 8). They adopted a differential pressure transducer and a capillary in series to the sample for the measure of the flow rate. Sadouki *et al.* (Sadouki et al., 2014) proposed a method to assess the value of the static viscous permeability based on the minimization of least-square numerical

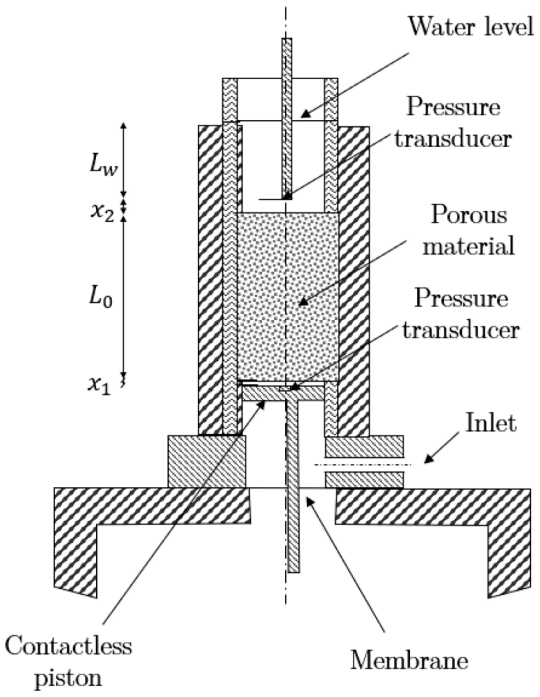

Fig. 8. Dynamic permeability measurement system: Smeulders et al. set up (Smeulders et al., 1992).

method using experimental transmitted waves in time domain.

3.1.3. Thermal and viscous characteristic lengths

Henry *et al.* (Henry et al., 1998) pointed out the possibility to estimate thermal characteristic length by using BET (Brunauer et al., 2002) techniques. Nevertheless, the BET technique yields large errors for typical acoustic material. Ultrasonic measurement set up may be a more efficient measurement method to assess the values of characteristic lengths. In the works of Leclaire *et al.* and Brown *et al.* (Leclaire et al., 1998; Leclaire et al., 1998; Leclaire et al., 1998; Brown et al., 1996), a method based on the utilizing the difference in physical properties of air and helium combining with high frequency limit of both viscous and thermal behaviour allows to evaluate the characteristic lengths. Due to linear behaviour of wavenumber at high frequencies (70–600 kHz), two slope, expressed in terms of Λ' and Λ, are obtained (Eq. (2), Ref. (Leclaire et al., 1998). Fohr *et al.* (Fohr et al., n.d.) carried out the measurement by positioning the sample between two ultrasonic transducers (40 kHz), one emitter and one receiver, as shown in Fig. 9. Two measures are carried out: with and without the tested samples. The relative time delay and amplitude attenuation caused by the tested material allow to extract both characteristic lengths and tortuosity (Eqs. (6) and (7), Ref. (Fohr et al., n.d.). Moussatov *et al.* and Ayrault *et al.* (Moussatov et al., 2001; Ayrault et al., 1999) carried out the measurements in a barometric chamber using a similar approach to Leclaire *et al.* (Leclaire et al., 1998). However, ultrasound techniques due to the attenuation of ultrasound propagation in the medium, are limited to lowly dissipative and thin materials.

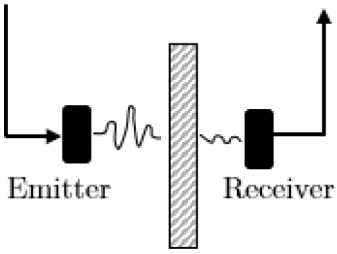

Fig. 9. Ultrasonic set up measurement (Fohr et al., n.d.).

3.1.4. High frequency limit of tortuosity

Allard *et al.* (Allard et al., 1998) provided an ultrasonic measurement technique to assess tortuosity of porous material based on the knowledge of the ratio of sound speed in the material and in free fluid at high frequency. It can be evaluated from the difference of the flight-time values of an ultrasonic pulse between two transducers with and without the material, see Fig. 9. Unmonva *et al.* and Fellah *et al.* (Umnova et al., 2005; Fellah et al., 2003) proposed a reflection and transmission coefficient-based method with ultrasound excitation to assess both porosity and tortuosity. In his work, Brown (Brown, 1980) pointed out the relation between electrical and acoustic properties of fluid-filled porous media at high frequency, where inertial forces dominate over the viscous ones. Furthermore, Brown proposed a non-acoustical direct method to measure tortuosity from the electrical resistivity of the porous material filled by an electrolyte. This is the reason why this methodology can only be applied for non-conductive frame. Furthermore, it can damage the material being tested.

3.1.5. Static thermal permeability

Henry and Allard and Debray *et al.* (Henry and Allard, 1997; Debray et al., 1998) showed an acoustic method to measure the trapping constant based on the low frequency limit of the bulk modulus (defined in terms of compressibility), see. Eq. (11) in Ref. (Debray et al., 1998). This method replaces Tarnow's acoustic set up (Tarnow, 1998) for the measurement of compressibility based on the variations of the resonance frequencies in a cylindrical tube with and without the testing sample, in Fig. 10. As for the static viscous permeability, Fellah *et al.* (Sadouki et al., 2011) provided an equivalent method based on temporal model of the direct and inverse scattering problem for the propagation in the porous material.

3.2. Indirect method

The indirect method is based on the works of Panneton and Olny (Olny and Panneton, 2008; Panneton and Olny, 2006), that provided inverse formulas to assess the transport parameters from the knowledge of dynamic thermal $\widetilde{K}$ and viscous $\widetilde{\rho}$ behaviour. These two dynamic quantities can be experimentally estimated from acoustical measurements with three- (Salissou et al., 2012)/four-microphones (Song and Bolton, 2000) techniques based on wave decomposition in impedance tube (Utsuno et al., 1998; ISO - ISO 10534-2:1998, 1998). An overview of these two measurement approaches is provided in Appendix A. Other thermoacoustic methodologies to assess the dynamic visco-thermal behaviour of porous material were proposed by Petculescu and Wilen, (Petculescu and Wilen, 2001; Wilen, 2001; Wilen, 1998). These techniques work especially well at low frequencies but require a dedicate instrumentation like a laser beam or a calibrated linear variable differential transformer (LVDT) to detect the displacement of the source.

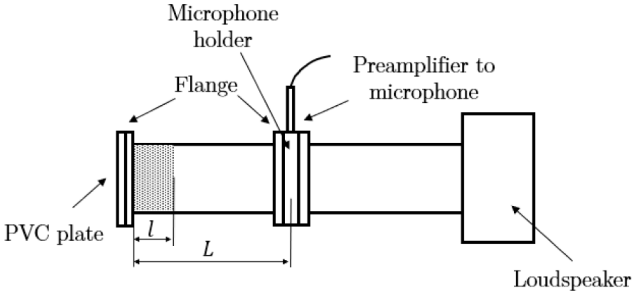

Fig. 10. Tarnow's acoustic set up for measure static thermal permeability (Tarnow, 1998).

Further low frequency techniques to assess the dynamic thermal $\widetilde{K}$ and viscous $\widetilde{\rho}$ have been derived by Napolitano *et al.* (Napolitano et al., 2022) and Di Giulio *et al.* (Di Giulio et al., 2022) based on lumped element hypothesis. These techniques require a simpler acoustic setup, consisting only in two microphones and a loudspeaker (reported in Appendix B).

The porosity can be estimated both from low and high frequency limit of dynamic bulk modulus as follow

$$\lim_{\omega\to 0}\widetilde{K}=\frac{P_0}{\varphi}, \tag{34}$$

$$\lim_{\omega\to+\infty}\widetilde{K}=\frac{\gamma P_0}{\varphi}. \tag{35}$$

At the same time, airflow resistivity can be obtained in the limit of low frequency of the imaginary part of dynamic density

$$\sigma=-\frac{1}{\varphi}\lim_{\omega\to 0}\Im(\omega\widetilde{\rho}). \tag{36}$$

Known these parameters, the others four are obtained from the provided analytical solutions

$$\alpha_\infty=\frac{1}{\rho_0}\left(\Re(\widetilde{\rho})-\sqrt{\Im(\widetilde{\rho})^2-\left(\frac{\sigma\varphi}{\omega}\right)^2}\right), \tag{37}$$

$$\Lambda=\alpha_\infty\sqrt{\frac{2\rho_0\mu}{\omega\Im(\widetilde{\rho})(\rho_0\alpha_\infty-\mathrm{Re}(\widetilde{\rho}))}}, \tag{38}$$

$$\Lambda'=\delta_\kappa\sqrt{2}\left\{-\Im\left[\left(\frac{\gamma P_0-\varphi\widetilde{K}}{\gamma P_0-\gamma\varphi\widetilde{K}}\right)^2\right]\right\}^{-\frac{1}{2}}, \tag{39}$$

$$k_0'=\frac{\varphi\delta_\kappa^2}{2}\left\{-\Re\left[\left(\frac{\gamma P_0-\varphi\widetilde{K}}{\gamma P_0-\gamma\varphi\widetilde{K}}\right)^2\right]\right\}^{-\frac{1}{2}}. \tag{40}$$

$\Re$ indicates the real part of a complex number. Eqs. (37) – (40) are valid in whole frequency range. Of course, the estimations of all the parameters are affected by uncertainties related to the impedance tube measurements (Jaouen et al., 2020; Doutres et al., 2010; Horoshenkov et al., 2007; Pompoli et al., 2017). In particular, as it can be seen the accuracy of the estimation of φ and σ influence the assessment of the other four parameters. Groby *et al.* (Groby et al., 2010) presented a similar method developed by Panneton and Olny (Olny and Panneton, 2008; Panneton and Olny, 2006) in the ultrasonic range. Based on the knowledge of scattering matrix and therefore of complex density and bulk modulus in high frequency range, Eqs. (17) and (18), porosity, tortuosity and characteristic lengths can be evaluated as follow

$$\Lambda=\delta_\nu\frac{\mathrm{Re}(\widetilde{\rho})-\mathrm{Im}(\widetilde{\rho})}{\mathrm{Im}(\widetilde{\rho})}, \tag{41}$$

$$\Lambda'=(1-\gamma)\delta_\kappa\frac{\mathrm{Re}\left(\widetilde{K}\right)-\mathrm{Im}\left(\widetilde{K}\right)}{\mathrm{Im}\left(\widetilde{K}\right)}, \tag{42}$$

$$\varphi=\frac{1}{\left|\widetilde{K}\right|}\left(1+(1-\gamma)\frac{2\delta_\kappa}{\Lambda'}+4(1-\gamma)^2\left(\frac{\delta_\kappa}{\Lambda'}\right)^2\right)^{\frac{1}{2}}, \tag{43}$$

$$\alpha_\infty=\varphi|\widetilde{\rho}|\left(1+\frac{2\delta_\nu}{\Lambda}+4\left(\frac{\delta_\nu}{\Lambda}\right)^2\right)^{-\frac{1}{2}}, \tag{44}$$

where $|\widetilde{\rho}|$ and $\left|\widetilde{K}\right|$ are respectively the absolute modulus of complex density and bulk modulus.

3.3. Inverse method

Inverse methods are essentially based on the minimization of cost function $C(\theta)$ in $\mathbb{R}^n$ space, θ is the set of n parameters that can be optimized by comparing experimental data and those provided by a theoretical model. Atalla and Panneton (Atalla and Raymond, n.d.) introduced this technique to assess the values of high frequency parameters $\theta=(\alpha_\infty,\Lambda,\Lambda')$ computing the JCA model (without considering k_0', equivalent to set $M'=1$). Taking as reference the surface impedance $\widetilde{Z}_s=-i\sqrt{\widetilde{K}\widetilde{\rho}}\cot\left(\omega\sqrt{\widetilde{K}/\widetilde{\rho}}\,d\right)$, with d the sample thickness, the cost function is defined as follow (Atalla and Raymond, n.d.)

$$C(\theta)=\frac{1}{2}\sum_{i=1}^{N}\left|\widetilde{Z}_{s_i,estimated}(\theta)-\widetilde{Z}_{s_i,observed}\right|^2, \tag{45}$$

where N is the total number of computed frequencies in the range of interest. Solution of the mathematical problem is found for $\theta^*=\{\alpha_\infty^*,\Lambda^*,\Lambda'^*\}$ for which $C(\theta^*)=\min[C(\theta)]$. Of course, in order to prevent local minima of $C(\theta)$ with no physical significance, upper and lower border constraints to values must be specified. Atalla and Panneton (Atalla and Raymond, n.d.) set the upper and lower bounds as

$$\begin{cases}1\le\alpha_\infty\le 4\\ \dfrac{1}{3.3}\left(\dfrac{8\alpha_\infty\mu}{\sigma\varphi}\right)^{\frac{1}{2}}\le(\Lambda,\Lambda')\le\dfrac{1}{3}\left(\dfrac{8\alpha_\infty\mu}{\sigma\varphi}\right)^{\frac{1}{2}}\\ \Lambda\le\Lambda'\end{cases}. \tag{46}$$

Further studies have been conducted to improve the inverse characterization methodology. Dragonetti *et al.* (Dragonetti et al., n.d.) highlighted the complex values of $\widetilde{Z}_s$ and proposed to find the minima of cost function in vector form dividing real and imaginary part

$$C(\theta^*)=\min\frac{1}{2}\sum_{i=1}^{N}\left(\begin{bmatrix}\mathrm{Re}\left(\widetilde{Z}_{s_i,estimated}(\theta)\right)\\ \mathrm{Im}\left(\widetilde{Z}_{s_i,estimated}(\theta)\right)\end{bmatrix}+\begin{bmatrix}\mathrm{Re}\left(\widetilde{Z}_{s_i,observed}\right)\\ \mathrm{Im}\left(\widetilde{Z}_{s_i,observed}\right)\end{bmatrix}\right)^2. \tag{47}$$

Chazot *et al.* and Roncen *et at.* (Chazot et al., 2012; Roncen et al., 2018) followed a Bayesian approach to assess the transport parameters and to quantify the uncertainties of each value though probability density functions. In that case, cost function comes out from a combination of data-fitting and a regularization term. Furthermore, Niskanen *et al.* (Niskanen et al., 2017) provided a twofold inversion characterization: a deterministic one (based on non-linear least squares) and a statistical one, to consider uncertainties on the parameters. Zielinski (Zieliński, 2015) choses a set of dimensionless parameters in order to render the

optimization algorithm robust and avoid problems of convergence due to different order of magnitude among transport parameters. Time domain inverse characterization approach has been provided by Fellah *et al.* (Fellah et al., 2007). Cost function is defined though reflected and transmitted pressure across the porous medium excited by ultrasound pulse

$$C(\theta) = \int_0^t p^r_{observed}(t) - p^r_{estimated}(\theta, t)dt + \int_0^t p^t_{observed}(t) - p^t_{estimated}(\theta, t)dt, \tag{48}$$

where p^r and p^t are respectively the reflected and transmitted signal. Initial values of parameters in the iterating process and boundary constraints can influence the convergence of the different algorithms to the minimization of cost functions. Two different approaches have been used: *Nonlinear best-fit* and *Genetic algorithms*. Comparison between different algorithms for inverse method and indirect calculation are reported in the paper provided by Bonfiglio and Pompoli (Bonfiglio and Pompoli, 2013). de Ryck *et al.* (de Ryck et al., 2008) applied a standard conjugate gradient method to reconstruct transport properties profiles $(\varphi(x), \alpha_\infty(x), \Lambda(x), \Lambda'(x), \sigma(x)$ where x is the direction of wave propagation) in inhomogeneous rigid frame material.

4. Numerical approaches

Numerical calculation of transport parameters is based on three uncoupled-steady problems:

(1) the Stokes flow problem, where viscous forces dominate over the inertial ones $(\omega \ll \omega_\nu)$ and static viscous permeability k_0 can be estimated;
(2) the Laplace's problem, where high frequency limit $(\omega \gg \omega_\nu)$ allows to consider the fluid inviscid and to calculate tortuosity α_∞ and characteristic lengths Λ, Λ';
(3) the Poisson's problem, which replaces the diffusion-controlled problem to assess static thermal permeability k'_0.

Each problem is defined in a Representative Elementary Volume (REV) of the material, identified by is the same in a Periodic Unit Cell constituting the porous media. The presented approach to assess transport parameters is generally called Hybrid Multiscale (HM) (Luu et al., 2017; Langlois et al., 2020; Perrot et al., 2008; Lee et al., 2009; Trinh et al., 2019; Chevillotte et al., 2010; Perrot et al., 2007; Luu et al., 2017; He et al., 2018; Perrot et al., 2011; Zieliński, 2014), while to achieve a complete dynamic description of the behaviour of material Direct Multiscale (DM) or Direct Numerical Simulation (DNS) approaches can be applied. An exhaustive synthesis of the computational approaches for modelling dynamic visco-thermal behaviour of porous material is reported in the work of Zielinski *et al.* (Zieliński et al., 2020). An example with the constitutive surfaces for the boundary conditions is reported in Fig. 11.

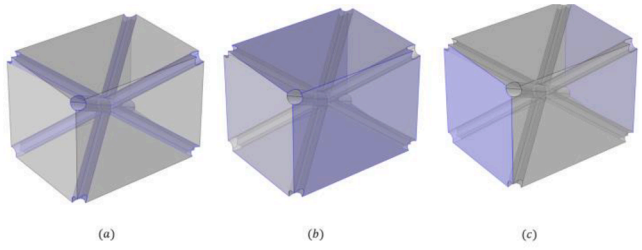

Fig. 11. Surface for the boundary conditions: (a) fluid–solid interface $\partial\Omega_{fs}$, (b) lateral surface $\partial\Omega_{lateral}$, (c) $\partial\Omega_{up}$ and $\partial\Omega_{dw}$.

4.1. Viscous flow

In the low Reynolds number, Stokes equation governs the behaviour of an incompressible Newtonian fluid

$$\mu\nabla^2 v - \nabla p = -G \text{ in } \Omega_f, \tag{49}$$

where the applied boundary conditions (BCs) are

$$\begin{cases} \nabla\cdot v = 0 & \text{in}\Omega_f \\ v = 0 & \text{on}\partial\Omega_{fs} \\ v\cdot n = 0 & \text{on}\partial\Omega_{lateral} \\ p = p_{up} & \text{on}\partial\Omega_{up} \\ p = p_{dw} & \text{on}\partial\Omega_{dw} \end{cases}. \tag{50}$$

p_{up} and p_{dw} are the pressures on the top (Ω_{up}) and bottom (Ω_{dw}) faces of the unit cell. Therefore, a macroscopic pressure gradient $G = \Delta p/L = p_{dw} - p_{up}$ is applied, with L the dimension of the cell in the direction of wave propagation. v is the velocity of fluid and no-slip boundary condition and periodicity are respectively applied to fluid–solid interface $(\partial\Omega_{fs})$ and lateral boundaries $(\partial\Omega_{f,lateral})$. The static viscous permeability can be evaluated from the averaged velocity over the fluid volume

$$k_0 = \mu\frac{\langle v\rangle\cdot e}{G} \tag{51}$$

where e is the unit vector of the direction of wave propagation.

4.2. Inertial flow

In high frequency range, viscous boundary layer becomes negligible compared to the cross-sectional size of the fluid flow section within the porous material, and the fluid behaves as an inviscid perfect one. According to Johnson *et al.*, Brown, Avellaneda and Torquato (Johnson et al., 1987; Brown, 1980; Avellaneda and Torquato, 1998; Cortis et al., 2003), this problem is equivalent to the problem of electric conduction, where the conducting fluid fills the porous media having a constant conductivity. Laplace's problem can be written as

$$\nabla^2\phi = 0 \text{ in } \Omega_f, \tag{52}$$

where BCs are

$$\begin{cases} \mathrm{E} = -\nabla\phi & \text{in}\Omega_f \\ \mathrm{E}\cdot n = 0 & \text{on}\partial\Omega_{lateral}\text{and}\partial\Omega_{fs} \\ \phi_{dw} = -\phi_{up} = -\Delta V/2 & \text{on}\partial\Omega_{up}\text{and}\partial\Omega_{dw} \end{cases}, \tag{53}$$

E and ϕ are respectively the local electric fields and the electric potential and they are Ω −periodic. Therefore, the high frequency limit of tortuosity and the viscous characteristic length can be evaluated as (Johnson et al., 1987; Cortis et al., 2003)

$$\alpha_\infty = \frac{\langle \mathrm{E}\cdot\mathrm{E}\rangle_{\Omega_f}}{\langle \mathrm{E}\rangle_{\Omega_f}\cdot\langle \mathrm{E}\rangle_{\Omega_f}}, \tag{54}$$

$$\Lambda = 2\frac{\int_{\Omega_f}\mathrm{E}\cdot\mathrm{E}\ dV}{\int_{\partial\Omega_f}\mathrm{E}\cdot\mathrm{E}\ dS}. \tag{55}$$

4.3. Thermal problem

Eq. (27), pointed out by Lafarge *et al.* (Lafarge et al., 1998), links the

Table 2
Uncoupled steady-problems and boundary conditions for transport parameters numerical evaluation.

	Ω_f	$\partial\Omega_w$	$\partial\Omega_{f,lateral}$	$\partial\Omega_{up}$	$\partial\Omega_{dw}$	Transport parameters
Stokes' problem	$\mu\nabla^2 v - \nabla p = -G\nabla\cdot v = 0$	$v = 0$	$v\cdot n = 0$	p_{up}	p_{dw}	$k_0 = \mu\frac{\langle v\rangle\cdot e}{G}$
Laplace's problem	$\nabla^2\phi = 0 E = -\nabla\phi$	$E\cdot n = 0$	$E\cdot n = 0$	ϕ_{up}	ϕ_{dw}	$\alpha_\infty = \frac{\langle \mathrm{E}\cdot\mathrm{E}\rangle_{\Omega_f}}{\langle \mathrm{E}\rangle_{\Omega_f}\cdot\langle \mathrm{E}\rangle_{\Omega_f}}\Lambda = 2\frac{\int_{\Omega_f}\mathrm{E}\cdot\mathrm{E}\, dV}{\int_{\partial\Omega_f}\mathrm{E}\cdot\mathrm{E}\, dS}$
Poisson's problem	$\nabla^2\tau = -1$	$\tau = 0$	$\nabla\tau\cdot n = 0$	$\nabla\tau\cdot n = 0$	$\nabla\tau\cdot n = 0$	$\varphi = \frac{\Omega_f}{\Omega_{tot}}\Lambda' = 2\frac{\Omega_f}{\partial\Omega_w}k_0' = \varphi\langle\tau\rangle$

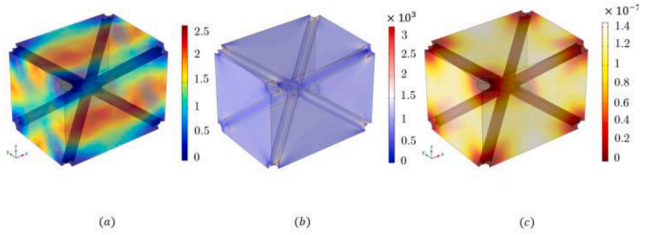

Fig. 12. Fields of the scaled velocity, electric potential, and temperature of tetragonal pin array unit cell.

acoustic fluctuations of temperature to the time derivative of acoustic pressure and the static thermal permeability is useful to describe thermal effects in the fluid saturating a solid skeleton, which can be considered as a thermostat. Furthermore, the Poisson's problem becomes

$$\nabla^2\tau = -1, \text{in}\,\Omega_f \tag{56}$$

where τ is Ω −periodic with boundary constraints

$$\begin{cases} \tau = 0 & \text{on}\partial\Omega_{fs} \\ \nabla\tau\cdot n = 0 & \text{on}\partial\Omega_{lateral}, \partial\Omega_{up}\text{and}\partial\Omega_{dw} \end{cases}. \tag{57}$$

Therefore, static thermal permeability is estimated as

$$k_0' = \varphi\langle\tau\rangle. \tag{58}$$

Porosity and thermal characteristic length are purely geometrical transport parameters not related to a specific physical field. Therefore, their values can be assessed only by using their definitions, Eqs. (24) and (28).

A synthesis of the boundary values problems involved in the evaluation of all the transport parameters is reported in Table 2. In Fig. 12, an example of the three scaled fields (velocity, electric potential, and temperature) is reported for a tetragonal pin array unit cell. It can be appreciated the increasing velocity in the lateral passage flow sections (Fig. 12.a), the periodicity of the electrical field on the lateral boundaries (Fig. 12.b) and the isothermal boundary condition imposed on the solid–fluid interfaces (Fig. 12.c).

4.4. Consistency of parameters

Considering their definitions, transport parameters are mutually independent; however, it is important to note that the geometry of the skeleton imposes constraints on the values they can assume. The viscous characteristic length is always lower than the thermal one (Johnson et al., 1987)

$$\Lambda \le \Lambda'. \tag{59}$$

At the same time, Avellaneda and Torquato (Avellaneda and Torquato, 1998) demonstrated the inequality between the static thermal and viscous permeability for all micro-geometries

$$k_0 \le k_0'. \tag{60}$$

Furthermore, for different typologies of material the tortuosity follows the Archie's empirical law (Archie, 1942)

$$\alpha_\infty = \left(\frac{1}{\varphi}\right)^r, \tag{61}$$

where r is a coefficient depending on the material. Another check can be done on the values of viscous and thermal pore shape factor M and M' which are of the order of magnitude around the unit for classical porous material for acoustic applications. For example, in case of uniform cross section materials, mathematical description of viscous and thermal problems has the same form (Stinson, 1998; Kozlov et al., 2005). Therefore, it results that (Lafarge et al., 1998)

$$\widetilde{k}(\omega) = \widetilde{k}'(P_r\omega) \tag{62}$$

$$M = M' \tag{63}$$

$$k_0 = k_0' \tag{64}$$

$$\Lambda = \Lambda' \tag{65}$$

$$\alpha_\infty = 1 \tag{66}$$

In Fig. 13 the dimensionless viscous and thermal permeabilities are reported in the case of straight circular pores (uniform cross-sectional material where $M = M' = 1$). As it can be seen, thermal and viscous

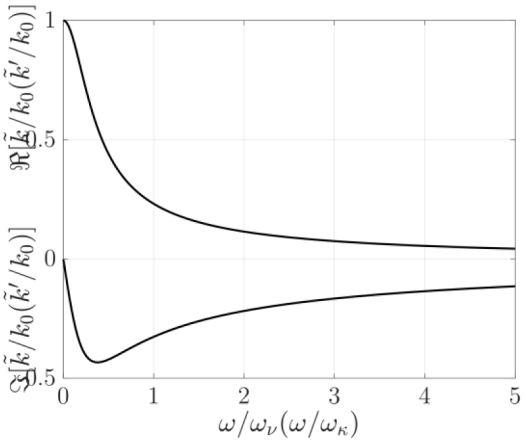

Fig. 13. Dimensionless viscous (thermal) permeability for straight cylindrical pores ($M = M' = 1, \alpha_\infty = 1, \varphi = 0.98$). It can be noted that scaled velocity and temperature fields have the same mathematical description.

Table 3
Literature's correlations for fibrous transport parameters.

Authors	Transport parameters	Description	Formula
Allard and Champoux (Allard and Champoux, 1998)	$\Lambda, \Lambda', \alpha_\infty,$	General fibrous	$\Lambda = \frac{1}{2\pi r_f L}\Lambda' = 2\Lambda\alpha_\infty = 1/\cos\beta$
Bies and Hansen (Bies and Hansen, 1980)	σ	General fibrous	$\sigma d_f^2 \rho_1^{-1.53} = \begin{cases} 3.18\times10^{-9}\text{Glass fibers} \\ 15.0\times10^{-9}\text{Polyester fibers} \end{cases}$
Lambert and Tesar (Lambert and Tesar, 1998)	k_0	General fibrous	$k_0 = \frac{d_f^2\varphi^3}{116.6\left[(1-\varphi)^2\right]}$
Tarnow (Tarnow, 1998)	k_0	Parallel (and transversal) squared (and random) fibers	$k_{0,PS} = \frac{b^2\left[\ln\left(\frac{1}{d_f}\right) - \frac{3}{2} + 2d_f\right]}{4\pi}$; $k_{0,PR} = \frac{b^2\left[1.28\ln\left(\frac{1}{d_f}\right) - 1.474 + 2d_f\right]}{4\pi}$ $k_{0,TS} = \frac{b^2\left[0.5\ln\left(\frac{1}{d_f}\right) - \frac{3}{4} + d_f - \frac{1}{4}{d_f}^2\right]}{4\pi}$; $k_{0,TR} = \frac{b^2\left[0.64\ln\left(\frac{1}{d_f}\right) - 0.737 + d_f\right]}{4\pi}$
Tamayol and Bahrami (Tamayol and Bahrami, 2010)	k_0	Parallel fibers in square, staggered and hexagonal arrangements	$k_0 = \frac{d_f^2}{16\varphi}\begin{cases} -1.479 - \ln\varphi + 2\varphi - \frac{\varphi^2}{2} - 0.0186\varphi^4 \\ -1.498 - \ln\varphi + 2\varphi - \frac{\varphi^2}{2} - 0.0018\varphi^6 \\ -1.352 - \ln\varphi + 2\varphi - \frac{\varphi^2}{2} - 0.2466\varphi^3 \end{cases}$
Tomadakis and Robertson (Tomadakis and Robertson, 2016)	k_0	One-, two-, and three-directional randomly overlapping fiber structures	$k_0 = \frac{d_f^2\varphi}{32\ln^2\varphi}\frac{(\varphi-\varepsilon)^{0.785+2}}{(1-\varepsilon)^{0.785}\left[(0.785+1)\varphi-\varepsilon\right]^2}$
Vallabh *et al.* (Vallabh et al., 2010)	k_0	General fibrous	$k_0 = (6.82e\times10^{-6})\frac{d_f}{1-\varphi} - 2.2\times10^{-11}\ln h + 1.64\times10^{-4}\frac{d_f}{(1-\varphi)^2} - 1.71\times10^{-9}(1-\varphi)6.66\times10^{-10}$
Koponen *et al.* (Koponen et al., 1998)	k_0, α_∞	General fibrous	$k_0 = \frac{d_f^2}{4}\frac{5.55}{e^{10.1(1-\varphi)}-1}\alpha_\infty = 1 + 0.65\frac{(1-\varphi)}{(\varphi-\varepsilon)^{0.19}}$
Rahli *et al.* (Rahli and Tadrist, 1995)	k_0	General fibrous	$k_0 = d_f\frac{62.5\varphi^6}{(1-\varphi)^2(3.6+56.4\varphi)^2}$
Davies (Davies, 2019)	k_0	General fibrous	$k_0 = \frac{d_f^2}{64(1-\varphi)^{\frac{3}{2}}\left(1+56(1-\varphi)^3\right)}$
Jackson and James (Jackson and James, 1986)	k_0	General fibrous	$k_0 = d_f^2\frac{3[-\ln(1-\varphi)-0.931]}{20(1-\varphi)}$
Ren *et al.* (Ren et al., 2017)	$\Lambda, \Lambda', \alpha_\infty, k_0, k_0', \varphi$	Metal fibers	See Table T1
Fotsing *et al.* (Fotsing et al., 2019)	$\Lambda, \Lambda', \alpha_\infty, k_0, \varphi$	Metal fibers	See Table T1
He *et al.* (He et al., 2022)	$\Lambda, \Lambda', \alpha_\infty, k_0$	Woven fibers	See Table T1
Di Giulio *et al.* (Di Giulio et al., 2023)	$\Lambda, \Lambda', \alpha_\infty, k_0, k_0', \varphi$	Wire Mesh	See Table T1
Luu *et al.* (Luu et al., 2017)	$\Lambda, \Lambda', \alpha_\infty, k_0, k_0', \varphi$	Fibers with orientation	See Table T1
Pompoli and Bonfiglio (Pompoli and Bonfiglio, 2020)	$\Lambda, \Lambda', \alpha_\infty, k_0, k_0', \varphi$	Fibers with orientation	See Table T1
Castagnéde *et al.* (Castagnède et al., 2000)	$\Lambda, \Lambda', \alpha_\infty, k_0, \varphi$	1D-/2D-compressed fibers	See Table T1
Lei *et al.* (Lei et al., 2018)	$\Lambda, \Lambda', \alpha_\infty, k_0, k_0', \varphi$	Compressed fibers with variation of angular orientation	See Table T1
Pompoli (Pompoli, 2023)	$\Lambda, \Lambda', \alpha_\infty, k_0, \varphi$	Poseidonian fibers	See Table T1

Table 4
Literature's correlations for granular materials transport parameters.

Authors	Transport parameters	Description	Formula
Boutin and Geidreau (Boutin and Geindreau, 2009; Boutin and Geindreau, 2010)	$\Lambda, \Lambda', \alpha_\infty$	Sphere and polyhedron packings	$\Lambda' = \frac{2\varphi\left[R(1-\varphi)^{\frac{1}{3}}\right]}{3(1-\varphi)}\Lambda = \frac{2\varphi(3-\varphi)\left[R(1-\varphi)^{\frac{1}{3}}\right]}{9(1-\varphi)}\alpha_\infty = \frac{3-\varphi}{2}$
Gasser et al. (Gasser et al., 2005)	Λ'	Face centered cubic sphere packing	$\Lambda' = 2\frac{(2R\sqrt{2})^3 - 4\left[\frac{4\pi R^3}{3} - 12\left(\pi h^2\left(R-\frac{h}{3}\right) - \pi r^2 h\right)\right]}{4\left[4\pi R^2 + 12(2\pi r h - 2\pi R h)\right]}h = R - \sqrt{R^2 - r^2}$
Zielinski (Zieliński, 2014)	$\Lambda, \Lambda', \alpha_\infty, k_0, k_0', \varphi$	Packed rigid spherical beads	See Table T1
Umnova et al. (Umnova et al., 2000; Umnova et al., 2001)	$\Lambda, \Lambda', \alpha_\infty, k_0, k_0', \varphi$	Packings of spheres	See Table T1
Tsuruha et al. (Tsuruha et al., 2020)	$\Lambda, \Lambda', \alpha_\infty, k_0$	Spherical granular material	$\alpha_\infty = 1 + \frac{1-\varphi}{2\varphi}k_0 = \frac{2\varphi^2 r^2\left(5 - 9\theta^{\frac{1}{3}} + 5\theta - \theta^2\right)}{45(1-\varphi)(1-\theta)}\Lambda = \frac{4(1-\theta)\varphi\alpha_\infty}{9(1-\varphi)}r\Lambda' = 2\frac{1-\varphi}{S_V}\theta = \frac{3(1-\varphi)}{\sqrt{2}\pi}$

Table 5
Literature's correlations for foam transport parameters.

Authors	Transport parameters	Description	Formula
Doutres et al. (Doutres et al., 2013; Doutres et al., 2014)	$\Lambda, \Lambda', \alpha_\infty, k_0, \varphi$	Polyurethane foams 3-/2-parameters model	See Table T1
Langlois et al. (Langlois et al., 2020)	$\Lambda, \Lambda', \alpha_\infty, k_0, k_0', \varphi$	Monodisperse foam	See Table T1
Perrot et al. (Perrot et al., 2011)	φ, Λ'	Open-cell foam (Kelvin cell)	$\varphi = 1 - \left(\frac{3\sqrt{2}\pi}{16}\right)\left(\frac{2r}{L}\right)^2 - \left(\frac{\sqrt{2}\pi C_1}{16}\right)\left(\frac{2r}{L}\right)^3 \Lambda' = r\frac{\frac{16\sqrt{2}}{\left(\frac{2r}{L}\right)^3} - \frac{6\pi}{\left(\frac{2r}{L}\right)} - 2\pi C_1}{3\pi\left(\frac{2}{\left(\frac{2r}{L}\right)} + C_2\right)} C_1 = -f^3 + 2\left(f^2-1\right)\sqrt{f^2-1}C_2 = -f^2 + 2(f-1)\sqrt{f^2-1} f = R/r$
Lee et al. (Lee et al., 2020)	$\Lambda, \Lambda', \alpha_\infty, k_0$	Polyurethane foam	See Table T1
Langlois et al. (Langlois et al., 2019)	α_∞, k_0	Solid foam	$k_0 = \frac{r_0^3}{3D_p}\left[n_{sq} + \frac{1}{2}n_{hex}\right] \alpha_\infty = \frac{\frac{\varphi}{4}}{\left(\frac{D_p}{2r_0} + \frac{h_m D_p}{\pi r_0^2}\right)\left(1 + 2.7\frac{r_0}{D_p} + 5.1\left(\frac{r_0}{D_p}\right)^2\right)}$

problems are represented in the same form. To have a complete description of boundary condition, isothermal condition of the solid skeleton $\left(T = 0 on \partial\Omega_{fs}\right)$ can be considered valid until the ratio

$$\epsilon_s = \frac{\rho_0 c_p \varphi}{\rho_s c_s (1-\varphi)} \ll 1, \tag{67}$$

where ρ_s and c_s are respectively the solid density and heat capacity. Further analysis on this thermal aspect at fluid–solid interface have been provided by Swift and Di Meglio *et al.* (Swift, 1998; Di Meglio et al., 2021), and a dynamic thermal third-type boundary condition has been developed. This condition takes into account both the temperature and the thermal flux at the solid–fluid interface.

5. Correlations for different types of materials

Analytical formulations to assess the transport parameters have been provided for different typologies of material, such as fibers, foams and granular are reported respectively in Table 3, Table 4, and Table 5. The complete set of JCAL correlations provided for various materials, and unit cells, is reported in Table T1.

5.1. Fibrous materials

For fibrous materials, several studies have been carried out to assess transport parameters. One of the first work of dynamic characterization of fibrous materials was provided by Attenborough (Attenborough, 1983). Attenborough's model is based on cylindrical-like pore assumption, where tortuosity $(\alpha_\infty = 1/\cos\beta)$ is related to the relative angle between cylindrical pores and the wave propagation direction β, and it is linked to the airflow resistivity and the porosity though a shape factor b.

Allard and Champoux (Allard and Champoux, 1998) provided semi-empirical relations to evaluate transport parameters of rigid frame fibrous materials in order to have an acoustic model which gives physical results also in low frequency regime. The model requires as input parameter the fiber diameter $d_f = 2r_f$, the material (fiber and air) bulk density ρ_b and the length per unit volume of the fibers $L = 4\rho_b/\pi d^2 \rho_m$ (said ρ_m the fiber density). Bies and Hansen (Bies and Hansen, 1980) developed a correlation between airflow resistivity, fibers diameter and the bulk density for different fibrous materials.

Further studies on the evaluation of the airflow resistivity have been realized by Lambert and Tesar and Tarnow (Lambert and Tesar, 1998; Tarnow, 1998; Tarnow, 1996), which provided correlations based also on the Kozeny-Carman relation:

$$k_0 = \frac{d_f^2 \varphi^3}{16C(1-\varphi)^2}, \tag{68}$$

with C is a constant value. Tarnow (Tarnow, 1996) suggested different correlations for square (S) and random (R) lattice displaced parallel (P) and transversal (T) to the acoustic wave direction.

Other analytical derivations of viscous permeability have been provided by Tamayol and Bahrami (Tamayol and Bahrami, 2009; Tamayol and Bahrami, 2010) for fibrous media in squared, staggered and hexagonal arrangements. A systematic study on viscous permeability of random fiber structures which considers mono-, bi- and three-dimensional arrangement of fibers and their overlapping is reported in the work of Tomadakis *et al.* (Tomadakis and Robertson, 2016). Also Vallabh *et al.*, Koponen *et al.*, Jackson and James and Davies (Vallabh et al., 2010; Koponen et al., 1998; Jackson and James, 1986; Davies, 2019; Rahli and Tadrist, 1995) highlighted different correlations for static viscous permeability for random fiber media, synthetized by Kerdudou (Kerdudou et al., 2021). Rigorous mathematical expressions for tortuosity and characteristic lengths of fibers have been derived by Umnova *et al.* (Umnova et al., 2009) for the high frequency asymptotic behaviour, and for airflow resistivity from low frequency regime. Simple formulations are given in the case of parallel (∥) and perpendicular (⊥) flow. Furthermore, thermal parameters are depending on the scalar temperature field that is not affected by the direction of propagation (Umnova et al., 2009). For viscous parameters, the dependency from velocity field determines their second-order tensor forms. Recently, Pompoli (Pompoli, 2023) provides a model to assess the transport parameters for Posidonia fibers based on loose fiber samples with different densities.

Computational approaches have been employed also for this kind of materials in the works of Luu *et al.*, He *et al.*, Peyrega and Jeulin (Luu et al., 2017; He et al., 2018; Luu et al., 2017; Peyrega and Jeulin, 2013). Luu *et al.* (Luu et al., 2017) provided correlations for transport parameters as function of porosity, fiber radius and fiber orientation, subsequently reviewed by Pompoli and Bonfiglio (Pompoli and Bonfiglio, 2020).

Effect of compression on transport parameters in fibrous materials has been highlighted by Castagnede *et al.* (Castagnède et al., 2000). Said $n = h_{(1)}/h_{(n)}$ the compression rate as the ratio between the uncompressed and the compressed thickness of material, the authors (Castagnède et al., 2000) pointed out the relations of 1D-compressed and 2D-compressed transport parameters with the uncompressed ones. Subsequently, other studies have been carried out also to evaluate the influence of compression on elastic frame (Wang et al., 2008; Kino and

Ueno, 2008; Kino, 2012; Hirosawa and Nakagawa, 2017). Lei *et al.* (Lei et al., 2018) provided correlation for compressed fibrous material taking into account the variation in fibers orientation during the compression, which modifies the viscous parameters instead of thermal ones which do not depend on the fibers' orientation.

Additive manufacturing technology has been employed to realize periodic acoustic structures of rigid micro-rods which can be schematized as sintered fibrous materials. Experimental studies and correlations for transport parameters are provided by Ren *et al.*, Fotsing *et al.,* He *et al.* and Di Giulio *et al.* (Ren et al., 2017; Fotsing et al., 2019; He et al., 2022; Di Giulio et al., 2023).

5.2. Granular materials

This kind of material is characterized by a lower porosity ($0.2 < \varphi < 0.6$) compared to the fibrous or foam one ($\varphi > 0.9$) (Saati et al., 2022). They are generally made by packaging of spheres which can be assembled in different cell structures (Boutin and Geindreau, 2009; Boutin and Geindreau, 2010; Zieliński, 2014; Gasser et al., 2005). Experimental characterization of transport parameters for random packings of beads was carried out by Allard *et al.* (Allard et al., 1998), with the techniques previously reported in Sec. 3. Attenborough (Attenborough, 1998) provided for these materials a model similar to the one for fibers. Transport parameters correlations for granular materials have been assessed by Umnova *et al.* (Umnova et al., 2000; Umnova et al., 2001), and then recalled in the work of Tsuruha *et al.* (Tsuruha et al., 2020).

Subsequently, Zielinski (Zieliński, 2014), based on the works of Boutin and Geindreau (Boutin and Geindreau, 2009; Boutin and Geindreau, 2010) on different boundary conditions in homogenization problem for packaging spheres, proposed geometric packings in order to achieve the value of the experimentally total porosity and gave correlations for each of the transport parameters, also as function of different BCs. As it can be seen from the Periodic Unit Cell, spheroidal beads have orthotropic behaviour and, as a result, the parallel and transversal components are maintained with respect to the wave propagation.

5.3. Cell-Foams materials

Cell-foams find application in different fields, from automotive to industry, because of their thermal, structural, and also acoustic properties. Numerous works (Langlois et al., 2020; Perrot et al., 2011; Doutres et al., 2013; Doutres et al., 2014; Doutres et al., 2011; Napolitano et al., 2017) point out the relation between microstructure of foams and their acoustic properties. Geometrical characterization of this kind of materials has been carried out by using 2D images from optical microscope or scanning electron microscope (SEM) or 3D reconstruction from X-ray tomography techniques (CT-scan) (Perrot et al., 2011; Doutres et al., 2011; Perrot et al., 2007; Lee et al., 2020). In the work of Doutres *et al.* (Doutres et al., 2011), the authors provided a 3-parameters (strut length l, strut thickness t, and reticulation rate R_w) semi-phenomenological model to predict the transport parameters. In a later work, Doutres *et al.* presented (Doutres et al., 2013) a simplified 2-parameters model, based on cell size C_s and reticulation rate R_w. From a computational point of view, numerical simulations have been carried out on Kelvin Unit Cell (tetrakaidecahedra unit-cell) in order to assess transport parameters from Hybrid Multiscale methodology (Langlois et al., 2020; Perrot et al., 2008; Trinh et al., 2019; Perrot et al., 2011). Based on the computational results, Langlois *et al.* (Langlois et al., 2020) gave a set of correlations for dimensionless transport parameters taking as reference length the Unit Cell dimension. Effects of membrane surface have been discussed in different works (Trinh et al., 2019; Tan Hoang and Perrot, 2012; Tan Hoang and Perrot, 2013). It results that, viscous parameters (Λ, k_0) decrease with the decreasing of the closure rate of membranes while thermal parameters slightly decrease. Therefore, the smaller the closure rate of membranes, the larger the ratios k_0'/k_0 and Λ'/Λ. Langlois *et al.* (Langlois et al., 2019) analysed the membrane effects of viscous fluid flow and electrical conductivity. Furthermore, the authors provided analytical estimates of viscous permeability as function of the ratio r_0/D_p, where r_0 is the radius of a perforated membrane and D_p the size of unit cell. Langlois *et al.* based their model on the analogy of pore connections (Sampson's law), considering also the number of squared n_{sq} and hexagonal n_{hex} perforated membrane. Kino *et al.* (Kino et al., 2009), based on his previous studies on fibrous materials, provided correlations new for transport parameters. His studies were carried out on compressed Illitech and Basotech melamine foam.

5.4. Other materials

Other than fibrous, granular and foam material, further typologies of micro-structures have been analysed in literature. Pin array lattice structure (Di Giulio et al., 2021; He et al., 2021; Horoshenkov et al., 2016; Horoshenkov et al., 2019; Auriault et al., 2010; Kirchhoff, 1868; Pompoli, 2023; Di Giulio et al., 2022) arranged in tetragonal body cell have been studied and correlations for non-acoustical parameters have been presented in terms of dimensionless cell size. He *at al.* (He et al., 2021) pointed out the influence of roughness of the sound absorption (then on transport parameters) by investigating on a petal-shaped micro channel. Horoshenkov *et al.* (Horoshenkov et al., 2019) underlined the possibility to predict acoustic behaviour of fibrous, foam and granular by using only three input parameters: the open porosity, the median pore size $\bar{s}$, standard deviation pore size σ_s. Furthermore, relations for each transport parameter as function of these three quantities are provided (Horoshenkov et al., 2019). Correlations for the complete set of transport parameters are synthetized in Table T1, with the respectively input terms for each model.

6. Conclusions

In this literature review, it was examined how experimental methods, numerical simulations, and analytical correlation may be used to evaluate the transport parameters. This could be helpful to researcher to choose the suitable micro-geometry for their specific application.

Furthermore, since additive manufacturing technology allows to realize porous materials with precise controlled geometries a key tool in the designing new micro-geometry of porous material, is also provided.

CRediT authorship contribution statement

Elio Di Giulio: Conceptualization, Formal analysis, Writing – original draft, Writing – review & editing. **Camille Perrot:** Resources, Supervision. **Raffaele Dragonetti:** Resources, Visualization, Writing – review & editing.

Declaration of competing interest

The authors declare that they have no known competing financial interests or personal relationships that could have appeared to influence the work reported in this paper.

Data availability

No data was used for the research described in the article.

Acknowledgments

The activities of Elio Di Giulio were supported by UniNA and Compagnia di San Paolo, in the framework of Programme STAR PLUS. Elio Di Giulio was on leave at University Gustave Eiffel from October the 1st of 2021 to March the 31st of 2022 thanks to a UNINA-DII fellowship (under the specific agreement between Université Gustave Eiffel and Università

degli Studi di Napoli Federico II number 2021/424).

Appendix A. Three- and four- microphones' techniques

In this appendix a shortly recall to characterized visco-thermal properties of porous material, in terms of complex density $\widetilde{\rho}$ and bulk modulus $\widetilde{K}$, is provided.

The measurement methods can be divided in to three- or four-microphones (Fig. A.1) techniques.

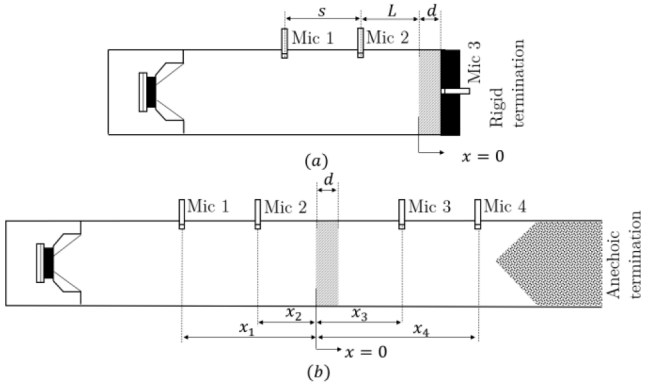

Fig. A1. (a) Three-microphones technique setup, (b) four-microphones technique setup.

Three microphones	Four microphones
$H_{12} = \frac{p_2}{p_1} A = \frac{i(p_1 e^{ikL} - p_2 e^{ik(L+s)})}{2\sin(ks)} B = \frac{i(p_2 e^{-ik(L+s)} - p_1 e^{-ikL})}{2\sin(ks)} p_0 = A + Br = \frac{H_{12} e^{iks} - 1}{1 - H_{12} e^{-iks}} e^{2ikL} H_{30} = \frac{p_0}{p_3} Z_s = \rho_0 c \frac{1+r}{1-r} \widetilde{k} = \frac{1}{d}\cos^{-1}(H_{30}) \widetilde{Z} = iZ_s \tan\left(\widetilde{k}d\right)$	$A = \frac{i(p_1 e^{ikx_2} - p_2 e^{ikx_1})}{2\sin(k(x_1 - x_2))} B = \frac{i(p_2 e^{-ikx_1} - p_1 e^{-ikx_2})}{2\sin(k(x_1 - x_2))} C = \frac{i(p_3 e^{ikx_4} - p_4 e^{ikx_3})}{2\sin(k(x_3 - x_4))} B = \frac{i(p_4 e^{-ikx_3} - p_3 e^{-ikx_4})}{2\sin(k(x_3 - x_4))} p_0 = A + B; v_0 = \frac{A - B}{\rho_0 c} p_d = Ce^{-ikd} + De^{ikd}; v_d = \frac{Ce^{-ikd} - De^{ikd}}{\rho_0 c} T_{11} = \frac{p_d v_d + p_0 v_0}{p_0 v_d + p_d v_0} T_{12} = \frac{p_0^2 - p_d^2}{p_0 v_d + p_d v_0} T_{21} = \frac{v_0^2 - v_d^2}{p_0 v_d + p_d v_0} \widetilde{k} = \frac{1}{d}\cos^{-1}(T_{11}) \widetilde{Z} = \sqrt{T_{12}/T_{21}}$

Once, the complex wavenumber $\widetilde{k}$ and the characteristic impedance $\widetilde{Z}$ are known, the complex density and bulk modulus can be evaluated from the relations:

$$\widetilde{\rho} = \frac{\varphi \widetilde{Z} \widetilde{k}}{\omega} \tag{A.1}$$

$$\widetilde{K} = \frac{\varphi \omega \widetilde{Z}}{\widetilde{k}}. \tag{A.2}$$

Appendix B. Acoustic lumped element techniques

This appendix reports a method to assess the bulk modulus and the complex density in the low frequencies range by using a lumped element hypothesis. The bulk modulus measurement setup relies for a rigid-end terminations, whereas the complex density measurements require an open-end, as it is shown respectively in Figs. B.1 and B.2. The measures of the viscous and the thermal dynamic properties of a tested sample are obtained from the acoustic pressures picked up by two microphones: one placed in the cavity behind the loudspeaker (p_{dw}), and one in the cavity where the sample is placed $\left(p_{up}\right)$:

$$\widetilde{\rho} = \varphi\left(\rho_m + \frac{\gamma p_m A}{\omega^2 V_{dw}(d - x_{mic})}\left[\left(\frac{p_{up}}{p_{dw}}\right)_{full} - \left(\frac{p_{up}}{p_{dw}}\right)_{empty}\right]\right), \tag{B.1}$$

$$\widetilde{K} = \frac{\gamma p_m}{\frac{1}{\varphi} - \frac{V_{dw}}{V_{up}\varphi}\left[\left(\frac{p_{up}}{p_{dw}}\right)_{full} - \left(\frac{p_{up}}{p_{dw}}\right)_{empty}\right]}, \tag{B.2}$$

where d and A are respectively the thickness and the cross-sectional area of the sample, x_{mic} is the microphone's position (relevant for the complex density measurement); V_{dw} and V_{up} are the lower and upper cavity volume. These techniques have a frequency validity range until $\left|\widetilde{k}d\right| < 0.5$, said $\widetilde{k} = \omega\sqrt{\frac{\widetilde{\rho}}{K}}$ the complex wavenumber of the material.

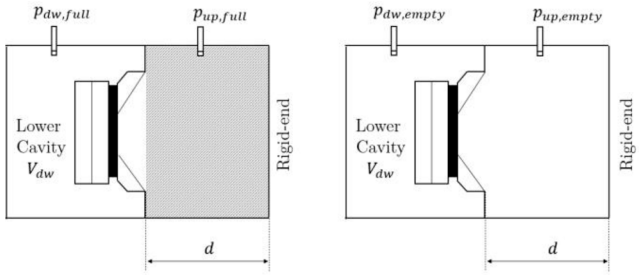

Fig. B1. The acoustic lumped element setup to measure the complex bulk modulus for the *full* configuration, on the left, and *empty* configuration, on the right.

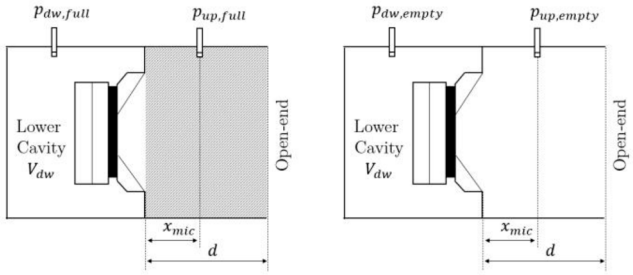

Fig. B2. The acoustic lumped element setup to measure the complex density for the *full* configuration, on the left, and *empty* configuration, on the right.

Appendix B. Supplementary data

Supplementary data to this article can be found online at https://doi.org/10.1016/j.ijheatfluidflow.2024.109426.

References

Allard, J.F., van Champoux, Y., 1998. New empirical equations for sound propagation in rigid frame fibrous materials, J. Acoust. Soc. Am. 91; 3346. 10.1121/1.402824.

Allard, J.F., Atalla, N., 2009. Propagation of Sound in Porous Media: Modelling Sound Absorbing Materials. John Wiley and Sons, 10.1002/9780470747339.

Allard, J.F., Castagnede, B., Henry, M., Lauriks, W., 1998. Evaluation of tortuosity in acoustic porous materials saturated by air. Rev. Sci. Instrum. 65, 754. https://doi.org/10.1063/1.1145097.

Allard, J.F., Henry, M., Tizianel, J., Kelders, L., Lauriks, W., 1998. Sound propagation in air-saturated random packings of beads. J. Acoust. Soc. Am. 104, 2004. https://doi.org/10.1121/1.423766.

American Society for Testing and Materials, E2611 - 09 - Standard Test Method for Measurement of Normal Incidence Sound Transmission of Acoustical Materials Based on the Transfer Matrix Method, 2017. 10.1520/E2611-09.

Archie, G.E., 1942. The electrical resistivity log as an aid in determining some reservoir characteristics. Trans. AIME 146, 54–62. https://doi.org/10.2118/942054-G.

Atalla, Y., Raymond, P., n.d. Inverse acoustical characterization of open cell porous media using impedance tube measurements, (n.d.). https://www.researchgate.net/publication/277101029_Inverse_acoustical_characterization_of_open_cell_porous_media_using_impedance_tube_measurements (accessed November 30, 2021).

Attenborough, K., 1983. Acoustical characteristics of rigid fibrous absorbents and granular materials. J. Acoust. Soc. Am. 73, 785–799. https://doi.org/10.1121/1.389045.

Attenborough, K., 1998. On the acoustic slow wave in air-filled granular media. J. Acoust. Soc. Am. 81, 93. https://doi.org/10.1121/1.394938.

Auriault, J.L., Borne, L., Chambon, R., 1998. Dynamics of porous saturated media, checking of the generalized law of Darcy. J. Acoust. Soc. Am. 77, 1641. https://doi.org/10.1121/1.391962.

Auriault, J.L., Boutin, C., Geindreau, C., 2010. Homogenization of Coupled Phenomena in Heterogenous Media. Wiley-ISTE. ISBN: 9781848211612. DOI: 10.1002/9780470612033.

Auriemma, F., Di Giulio, E., Napolitano, M., Dragonetti, R. 2020. Porous cores in small thermoacoustic devices for building applications, Energies, 13; 2941. 10.3390/EN13112941.

Auriemma, F., Holovenko, Y., 2019. Performance of additive manufactured stacks in a small scale thermoacoustic heat engine. SAE Technical Papers. https://doi.org/10.4271/2019-01-1534.

Avellaneda, M., Torquato, S., 1998. Rigorous link between fluid permeability, electrical conductivity, and relaxation times for transport in porous media. Phys. Fluids A 3, 2529. https://doi.org/10.1063/1.858194.

Ayrault, C., Moussatov, A., Castagnède, B., Lafarge, D., 1999. Ultrasonic characterization of plastic foams via measurements with static pressure variations. Appl. Phys. Lett. 74, 3224. https://doi.org/10.1063/1.124112.

Beranek, L.L., 2005. Acoustic impedance of porous materials. J. Acoust. Soc. Am. 13, 248. https://doi.org/10.1121/1.1916172.

Bies, D.A., Hansen, C.H., 1980. Flow resistance information for acoustical design. Appl. Acoust. 13, 357–391. https://doi.org/10.1016/0003-682X(80)90002-X.

Biot, M.A., 1956. Theory of propagation of elastic waves in a fluid-saturated porous solid. I. Low-frequency range. J. Acoust. Soc. Am. 28, 168–178. https://doi.org/10.1121/1.1908239.

Biot, M.A., 2005. Theory of propagation of elastic waves in a fluid-saturated porous solid. II. Higher frequency range. J. Acoust. Soc. Am. 28, 179. https://doi.org/10.1121/1.1908241.

Bonfiglio, P., Pompoli, F., 2013. Inversion problems for determining physical parameters of porous materials: Overview and comparison between different methods. Acta Acust. Acust. 99, 341–351. https://doi.org/10.3813/AAA.918616.

Boutin, C., Geindreau, C., 2009. Estimates and bounds of dynamic permeability of granular media. J. Acoust. Soc. Am. 124, 3576. https://doi.org/10.1121/1.2999050.

Boutin, C., Geindreau, C., 2010. Periodic homogenization and consistent estimates of transport parameters through sphere and polyhedron packings in the whole porosity range. Phys. Rev. E Stat. Nonlin. Soft Matter Phys. 82, 036313 https://doi.org/10.1103/PHYSREVE.82.036313/FIGURES/18/MEDIUM.

Brown, R.J.S., 1980. Connection between formation factor for electrical resistivity and fluid-solid coupling factor in Biot's equations for acoustic waves in fluid-filled porous media. Geophysics 45, 1269–1275. https://doi.org/10.1190/1.1441123.

Brown, R.L., Bolt, R.H., 2005. The measurement of flow resistance of porous acoustic materials. J. Acoust. Soc. Am. 13, 337. https://doi.org/10.1121/1.1916184.

Brown, N., Melon, M., Montembault, V., Castagnede, B., Lauriks, W., Leclaire, P., 1996. Evaluation of the viscous characteristic length of air-saturated porous materials from the ultrasonic dispersion curve. accessed November 30, 2021 Comptes Rendus de l'Académie Des Sciences Série IIb, Mécanique 322, 122–127. https://hal.archives-ouvertes.fr/hal-01326811.

Brunauer, S., Emmett, P.H., Teller, E., 2002. Adsorption of gases in multimolecular layers. J. Am. Chem. Soc. 60, 309–319. https://doi.org/10.1021/JA01269A023.

Castagnède, B., Aknine, A., Brouard, B., Tarnow, V., 2000. Effects of compression on the sound absorption of fibrous materials. Appl. Acoust. 61, 173–182. https://doi.org/10.1016/S0003-682X(00)00003-7.

Champoux, Y., Allard, J., 1998. Dynamic tortuosity and bulk modulus in air-saturated porous media. J. Appl. Phys. 70, 1975. https://doi.org/10.1063/1.349482.

Champoux, Y., Stinson, M.R., Daigle, G.A., 1998. Air-based system for the measurement of porosity. J. Acoust. Soc. Am. 89, 910. https://doi.org/10.1121/1.1894653.

Charlaix, E., Kushnick, A.P., Stokes, J.P., 1988. Experimental study of dynamic permeability in porous media. Phys. Rev. Lett. 61, 1595. https://doi.org/10.1103/PhysRevLett.61.1595.
Chazot, J.-D., Zhang, E., Antoni, J., 2012. Acoustical and mechanical characterization of poroelastic materials using a Bayesian approach. J. Acoust. Soc. Am. 131, 4584. https://doi.org/10.1121/1.3699236.
Chevillotte, F., Panneton, R., Perrot, C., 2010. Microstructure based model for sound absorption predictions of perforated closed-cell metallic foams. J. Acoust. Soc. Am. 128, 1766. https://doi.org/10.1121/1.3473696.
Cortis, A., Smeulders, D.M.J., Guermond, J.L., Lafarge, D., 2003. Influence of pore roughness on high-frequency permeability. Phys. Fluids 15, 1766. https://doi.org/10.1063/1.1571545.
Davies, C.N. 2019. The separation of airborne dust and particles, 167:185–213. 10.1177/000203483531670 1B13.
de Ryck, L., Lauriks, W., Leclaire, P., Groby, J.P., Wirgin, A., Depollier, C., 2008. Reconstruction of material properties profiles in one-dimensional macroscopically inhomogeneous rigid frame porous media in the frequency domain. J. Acoust. Soc. Am. 124, 1591. https://doi.org/10.1121/1.2959734.
Debray, A., Allard, J.F., Lauriks, W., Kelders, L., 1998. Acoustical measurement of the trapping constant of porous materials. Rev. Sci. Instrum. 68, 4462. https://doi.org/10.1063/1.1148414.
Delany, M.E., Bazley, E.N., 1970. Acoustical properties of fibrous absorbent materials. Appl. Acoust. 3, 105–116. https://doi.org/10.1016/0003-682X(70)90031-9.
di Giulio, E., Auriemma, F., Napolitano, M., Dragonetti, R., 2021. Acoustic and thermoacoustic properties of an additive manufactured lattice structurea). J. Acoust. Soc. Am. 149, 3878. https://doi.org/10.1121/10.0005085.
Di Giulio, E., Auriemma, F., Napolitano, M., Dragonetti, R., 2021. Acoustic and thermoacoustic properties of an additive manufactured lattice structure. J. Acoust. Soc. Am. 149, 3878–3888. https://doi.org/10.1121/10.0005085.
Di Giulio, E., Napolitano, M., Di Meglio, A., Romano, R.A., Dragonetti, R., 2022. Low frequency acoustic method to measure the complex density of porous materials. J. Acoust. Soc. Am. 152, 2220. https://doi.org/10.1121/10.0014762.
Di Giulio, E., Di Meglio, A., Massarotti, N., Dragonetti, R., 2022. Effective thermal conductivity model for tetragonal pin array stack. J. Fluid Flow Heat Mass Transf. https://doi.org/10.11159/jffhmt.2022.005.
Di Giulio, E., Nguyen, C.T., Perrot, C., Dragonetti, R., 2023. Wire mesh stack and regenerator model for thermoacoustic devices. Appl. Therm. Eng. 221, 119816 https://doi.org/10.1016/j.applthermaleng.2022.119816.
Di Meglio, A., Di Giulio, E., Dragonetti, R., Massarotti, N., 2021. Analysis of heat capacity ratio on porous media in oscillating flow. Int. J. Heat Mass Transf. 179, 121724 https://doi.org/10.1016/j.ijheatmasstransfer.2021.121724.
Di Meglio, A., Di Giulio, E., Dragonetti, R., Massarotti, N., 2022. A novel model for macroscopic simulation of oscillating heat and fluid flow in porous media. Int. J. Therm. Sci. 181, 107758 https://doi.org/10.1016/j.ijthermalsci.2022.107758.
Doutres, O., Salissou, Y., Atalla, N., Panneton, R., 2010. Evaluation of the acoustic and non-acoustic properties of sound absorbing materials using a three-microphone impedance tube. Appl. Acoust. 71, 506–509. https://doi.org/10.1016/J.APACOUST.2010.01.007.
Doutres, O., Atalla, N., Dong, K., 2011. Effect of the microstructure closed pore content on the acoustic behavior of polyurethane foams. J. Appl. Phys. 110, 064901 https://doi.org/10.1063/1.3631021.
Doutres, O., Atalla, N., Dong, K., 2013. A semi-phenomenological model to predict the acoustic behavior of fully and partially reticulated polyurethane foams. J. Appl. Phys. 113, 054901 https://doi.org/10.1063/1.4789595.
Doutres, O., Ouisse, M., Atalla, N., Ichchou, M., 2014. Impact of the irregular microgeometry of polyurethane foam on the macroscopic acoustic behavior predicted by a unit-cell model. J. Acoust. Soc. Am. 136, 1666–1681. https://doi.org/10.1121/1.4895695.
Dragonetti, R., Ianniello, C., Romano, R.A. n.d. The evaluation of intrinsic non-acoustic parameters of polyester fibrous materials by an optimization procedure, (n.d.). https://www.researchgate.net/publication/273490912_The_evaluation_of_intrinsic_non-acoustic_parameters_of_polyester_fibrous_materials_by_an_optimization_procedure (accessed November 30, 2021).
Dragonetti, R., Ianniello, C., Romano, R.A., 2011. Measurement of the resistivity of porous materials with an alternating air-flow method. J. Acoust. Soc. Am. 129, 753. https://doi.org/10.1121/1.3523433.
Dragonetti, R., Napolitano, M., Di Filippo, S., Romano, R., 2016. Modeling energy conversion in a tortuous stack for thermoacostic applications. Appl. Therm. Eng. 103, 233–242. https://doi.org/10.1016/J.APPLTHERMALENG.2016.04.076.
Fellah, Z.E.A., Berger, S., Lauriks, W., Depollier, C., Fellah, M., 2002. Measuring the porosity of porous materials having a rigid frame via reflected waves: A time domain analysis with fractional derivatives. J. Appl. Phys. 93, 296. https://doi.org/10.1063/1.1524025.
Fellah, Z.E.A., Berger, S., Lauriks, W., Depollier, C., Aristégui, C., Chapelon, J.-Y., 2003. Measuring the porosity and the tortuosity of porous materials via reflected waves at oblique incidence. J. Acoust. Soc. Am. 113, 2424. https://doi.org/10.1121/1.1567275.
Fellah, Z.E.A., Mitri, F.G., Fellah, M., Ogam, E., Depollier, C., 2007. Ultrasonic characterization of porous absorbing materials: Inverse problem. J. Sound Vib. 302, 746–759. https://doi.org/10.1016/J.JSV.2006.12.007.
Fohr, F., Parmentier, D., Castagnede, B.R.J., Henry, M. n.d., An alternative and industrial method using low frequency ultrasound enabling to measure quickly tortuosity and viscous characteristic length.
Fotsing, E.R., Dubourg, A., Ross, A., Mardjono, J., 2019. Acoustic properties of periodic micro-structures obtained by additive manufacturing. Appl. Acoust. 148, 322–331. https://doi.org/10.1016/J.APACOUST.2018.12.030.
Gasser, S., Paun, F., Bréchet, Y., 2005. Absorptive properties of rigid porous media: Application to face centered cubic sphere packing. J. Acoust. Soc. Am. 117, 2090. https://doi.org/10.1121/1.1863052.
Groby, J.-P., Ogam, E., de Ryck, L., Sebaa, N., Lauriks, W., 2010. Analytical method for the ultrasonic characterization of homogeneous rigid porous materials from transmitted and reflected coefficients. J. Acoust. Soc. Am. 127, 764. https://doi.org/10.1121/1.3283043.
He, W., Liu, M., Peng, X., Xin, F., Lu, T.J., 2021. Sound absorption of petal shaped micro-channel porous materials. Phys. Fluids 33, 063606. https://doi.org/10.1063/5.0053059.
He, W., Peng, X., Xin, F., Lu, T.J., 2022. A microstructure-based model of transport parameters and sound absorption for woven fabrics. Compos. Sci. Technol. 227, 109607 https://doi.org/10.1016/J.COMPSCITECH.2022.109607.
He, M., Perrot, C., Guilleminot, J., Leroy, P., Jacqus, G., 2018. Multiscale prediction of acoustic properties for glass wools: Computational study and experimental validation. J. Acoust. Soc. Am. 143, 3283. https://doi.org/10.1121/1.5040479.
Henry, M., Allard, J.F., 1997. Acoustical measurement of the trapping constant of foams with open cells, Comptes Rendus de l'Académie Des Sciences - Series IIB - Mechanics-Physics-Chemistry-Astronomy 325; 331–338. 10.1016/S1251-8069(97)81151-7.
Henry, M., Lemarinier, P., Allard, J.F., Bonardet, J.L., Gedeon, A., 1998. Evaluation of the characteristic dimensions for porous sound-absorbing materials. J. Appl. Phys. 77, 17. https://doi.org/10.1063/1.359366.
Hirosawa, K., Nakagawa, H., 2017. Formulae for predicting non-acoustical parameters of deformed fibrous porous materials. J. Acoust. Soc. Am. 141, 4301–4313. https://doi.org/10.1121/1.4984291.
Horoshenkov, K.V., Khan, A., Bécot, F.-X., Jaouen, L., Sgard, F., Renault, A., Amirouche, N., Pompoli, F., Prodi, N., Bonfiglio, P., Pispola, G., Asdrubali, F., Hübelt, J., Atalla, N., Amédin, C.K., Lauriks, W., Boeckx, L., 2007. Reproducibility experiments on measuring acoustical properties of rigid-frame porous media (round-robin tests). J. Acoust. Soc. Am. 122, 345. https://doi.org/10.1121/1.2739806.
Horoshenkov, K.V., Groby, J.-P., Dazel, O., 2016. Asymptotic limits of some models for sound propagation in porous media and the assignment of the pore characteristic lengths. J. Acoust. Soc. Am. 139, 2463. https://doi.org/10.1121/1.4947540.
Horoshenkov, K.V., Hurrell, A., Groby, J.-P., 2019. A three-parameter analytical model for the acoustical properties of porous media. J. Acoust. Soc. Am. 145, 2512–2517. https://doi.org/10.1121/1.5098778.
Ingard, K.U., Dear, T.A., Ingard, K.U., Dear, T.A., 1985. Measurement of acoustic flow resistance. JSV 103, 567–572. https://doi.org/10.1016/S0022-460X(85)80024-9.
ISO - ISO 10534-2:1998 - Acoustics — Determination of sound absorption coefficient and impedance in impedance tubes — Part 2: Transfer-function method, (n.d.). https://www.iso.org/standard/22851.html (accessed November 30, 2021).
ISO - ISO 9053-1:2018 - Acoustics — Determination of airflow resistance — Part 1: Static airflow method, (n.d.). https://www.iso.org/standard/69869.html (accessed November 30, 2021).
ISO - ISO 9053-2:2020 - Acoustics — Determination of airflow resistance — Part 2: Alternating airflow method, (n.d.). https://www.iso.org/standard/76744.html (accessed November 30, 2021).
Jackson, G.W., James, D.F., 1986. The permeability of fibrous porous media. Can. J. Chem. Eng. 64, 364–374. https://doi.org/10.1002/CJCE.5450640302.
Jaouen, L., Gourdon, E., Glé, P., Gl, P., 2020. Estimation of all six parameters of Johnson-Champoux-Allard-Lafarge model for acoustical porous materials from impedance tube measurements. J. Acoust. Soc. Am. 148, 1998. https://doi.org/10.1121/10.0002162.
Johnson, D.L., Koplik, J., Dashen, R., 1987. Theory of dynamic permeability and tortuosity in fluid-saturated porous media. J. Fluid Mech. 176, 379–402. https://doi.org/10.1017/S0022112087000727.
Kerdudou, P., Chéné, J. G.J.-T. 44th I., 2015, A semi-empirical approach to link macroscopic parameters to microstructure of fibrous materials, Researchgate.Net (n.d.). https://www.researchgate.net/profile/Gary-Jacqus/publication/280297586_A_semi-empirical_approach_to_link_macroscopic_parameters_to_microstructure_of_fibrous_materials/links/55aff5b908ae32092e06faf2/A-semi-empirical-approach-to-link-macroscopic-parameters-to-microstructure-of-fibrous-materials.pdf (accessed December 1, 2021).
Kino, N., 2012. A comparison of two acoustical methods for estimating parameters of glass fibre and melamine foam materials. Appl. Acoust. 73, 590–603. https://doi.org/10.1016/J.APACOUST.2011.12.007.
Kino, N. Ueno, T., 2008. Comparisons between characteristic lengths and fibre equivalent diameters in glass fibre and melamine foam materials of similar flow resistivity, Appl. Acoust. https://www.sciencedirect.com/science/article/pii/S0003682X06002325 (accessed December 1, 2021).
Kino, N., Ueno, T., Suzuki, Y., Makino, H., 2009. Investigation of non-acoustical parameters of compressed melamine foam materials. Appl. Acoust. 70, 595–604. https://doi.org/10.1016/J.APACOUST.2008.07.002.
Kirchhoff, G. 1868. Ueber den Einfluss der Wärmeleitung in einem Gase auf die Schallbewegung. In: Annalen der Physik 210.6, pp. 177–193. ISSN: 1521-3889. DOI: 10.1002/ANDP.18682100602.
Koponen, A., Kandhai, D., Hellén, E., Alava, M., Hoekstra, A., Kataja, M., Niskanen, K., Sloot, P., Timonen, J., 1998. Permeability of three-dimensional random fiber webs. Phys. Rev. Lett. 80, 716. https://doi.org/10.1103/PhysRevLett.80.716.
Kozlov, V.F., Fedorov, A. v., Malmuth, N.D. 2005. Acoustic properties of rarefied gases inside pores of simple geometries, J. Acoust. Soc. Am. 117;3402. 10.1121/1.1893428.
Lafarge, D., Lemarinier, P., Allard, J.F., Tarnow, V., 1998. Dynamic compressibility of air in porous structures at audible frequencies. J. Acoust. Soc. Am. 102, 1995. https://doi.org/10.1121/1.419690.

Lambert, R.F., Tesar, J.S., 1998. Acoustic structure and propagation in highly porous, layered, fibrous materials. J. Acoust. Soc. Am. 76, 1231. https://doi.org/10.1121/1.391417.
Langlois, V., Trinh, V.H., Perrot, C., 2019. Electrical conductivity and tortuosity of solid foam: Effect of pore connections. Phys. Rev. E 100, 013115. https://doi.org/10.1103/PHYSREVE.100.013115/FIGURES/15/MEDIUM.
Langlois, V., Kaddami, A., Pitois, O., Perrot, C., 2020. Acoustics of monodisperse open-cell foam: An experimental and numerical parametric study. J. Acoust. Soc. Am. 148, 1767. https://doi.org/10.1121/10.0001995.
Leclaire, P., Kelders, L., Lauriks, W., Melon, M., Brown, N., Castagnède, B., 1998. Determination of the viscous and thermal characteristic lengths of plastic foams by ultrasonic measurements in helium and air. J. Appl. Phys. 80, 2009. https://doi.org/10.1063/1.363817.
Leclaire, P., Kelders, L., Lauriks, W., Glorieux, C., Thoen, J., 1998. Determination of the viscous characteristic length in air-filled porous materials by ultrasonic attenuation measurements. J. Acoust. Soc. Am. 99, 1944. https://doi.org/10.1121/1.415378.
Leclaire, P., Kelders, L., Lauriks, W., Allard, J.F., Glorieux, C., 1998. Ultrasonic wave propagation in reticulated foams saturated by different gases: High frequency limit of the classical models. Appl. Phys. Lett. 69, 2641. https://doi.org/10.1063/1.117544.
Leclaire, P., Umnova, O., Horoshenkov, K.V., Maillet, L., 2003. Porosity measurement by comparison of air volumes. Rev. Sci. Instrum. 74, 1366. https://doi.org/10.1063/1.1542666.
Lee, C.-Y., Leamy, M.J., Nadler, J.H., 2009. Acoustic absorption calculation in irreducible porous media: A unified computational approach. J. Acoust. Soc. Am. 126, 1862. https://doi.org/10.1121/1.3205399.
Lee, H.R., Yang, S.S., Lee, J.W., Kang, Y.J., 2020. Estimation and uncertainty analysis of fluid-acoustic parameters of porous materials using microstructural properties. J. Acoust. Soc. Am. 148, 308. https://doi.org/10.1121/10.0001580.
Lei, L., Dauchez, N., Chazot, J.D., 2018. Prediction of the six parameters of an equivalent fluid model for thermocompressed glass wools and melamine foam. Appl. Acoust. 139, 44–56. https://doi.org/10.1016/J.APACOUST.2018.04.010.
Leonard, R.W., 2005. Simplified flow resistance measurements. J. Acoust. Soc. Am. 17, 240. https://doi.org/10.1121/1.1916323.
Liu, J., Garrett, S.L., 2006. Relationship between Nusselt number and the thermoviscous (Rott) functions. J. Acoust. Soc. Am. 119, 1457. https://doi.org/10.1121/1.2165000.
Lu, G., Cheng, P., 2012. Friction factor and Nusselt number for thermoacoustic transport phenomena in a tube, 14; 566–573. 10.2514/2.6558.
Luu, H.T., Perrot, C., Panneton, R., 2017. Influence of Porosity, Fiber Radius and Fiber Orientation on the Transport and Acoustic Properties of Random Fiber Structures, Acta Acustica United with. Acust. 103, 1050–1063. https://doi.org/10.3813/AAA.919134.
Luu, H.T., Perrot, C., Monchiet, V., Panneton, R., 2017. Three-dimensional reconstruction of a random fibrous medium: Geometry, transport, and sound absorbing properties. J. Acoust. Soc. Am. 141, 4768–4780. https://doi.org/10.1121/1.4989373.
Luu, H.T., Panneton, R., Perrot, C., 2017. Effective fiber diameter for modeling the acoustic properties of polydisperse fiber networks. J Acoust Soc Am 141 EL96–EL101. https://doi.org/10.1121/1.4976114.
Miki, Y., 1990. Acoustical properties of porous materials-Modifications of Delany-Bazley models. J. Acoust. Soc. Japan (E) 11, 19–24. https://doi.org/10.1250/AST.11.19.
Moussatov, A., Ayrault, C., Castagnède, B., 2001. Porous material characterization – ultrasonic method for estimation of tortuosity and characteristic length using a barometric chamber. Ultrasonics 39, 195–202. https://doi.org/10.1016/S0041-624X(00)00062-7.
Napolitano, M., Romano, R., Dragonetti, R., 2017. Open-cell foams for thermoacoustic applications. Energy 138, 147–156. https://doi.org/10.1016/J.ENERGY.2017.07.042.
Napolitano, M., Di Giulio, E., Auriemma, F., Romano, R.A., Dragonetti, R., 2022. Low frequency acoustic method to measure the complex bulk modulus of porous materials. J. Acoust. Soc. Am. 151, 1545–1556. https://doi.org/10.1121/10.0009767.
Niskanen, M., Groby, J.-P., Duclos, A., Dazel, O., le Roux, J.C., Poulain, N., Huttunen, T., Lähivaara, T., 2017. Deterministic and statistical characterization of rigid frame porous materials from impedance tube measurements. J. Acoust. Soc. Am. 142, 2407. https://doi.org/10.1121/1.5008742.
Olny, X., Panneton, R., 2008. Acoustical determination of the parameters governing thermal dissipation in porous media. J. Acoust. Soc. Am. 123, 814. https://doi.org/10.1121/1.2828066.
Panneton, R., Olny, X., 2006. Acoustical determination of the parameters governing viscous dissipation in porous media. J. Acoust. Soc. Am. 119, 2027. https://doi.org/10.1121/1.2169923.
Perrot, C., Panneton, R., Olny, X., 2007. Computation of the dynamic thermal dissipation properties of porous media by Brownian motion simulation: Application to an open-cell aluminum foam. J. Appl. Phys. 102, 074917 https://doi.org/10.1063/1.2786899.
Perrot, C., Panneton, R., Olny, X., 2007. Periodic unit cell reconstruction of porous media: Application to open-cell aluminum foams. J. Appl. Phys. 101, 113538 https://doi.org/10.1063/1.2745095.
Perrot, C., Chevillotte, F., Panneton, R., Allard, J.-F., Lafarge, D., 2008. On the dynamic viscous permeability tensor symmetry. J Acoust Soc Am 124, EL210. https://doi.org/10.1121/1.2968300.
Perrot, C., Chevillotte, F., Panneton, R., 2008. Dynamic viscous permeability of an open-cell aluminum foam: Computations versus experiments. J. Appl. Phys. 103 https://doi.org/10.1063/1.2829774.
Perrot, C., Bonnet, G., Hoang, M.T., Chevillotte, F., Bécot, F.-X., Gautron, L., Duval, A., Hoang, M.T., Chevillotte, F., Bécot, F.-X., Duval, A., 2011. Microstructure, transport, and acoustic properties of open-cell foam samples. Phys. Acoust. Paper # 2019-R36 https://hal-upec-upem.archives-ouvertes.fr/hal-00732572 (accessed December 1, 2021).
Petculescu, A., Wilen, L.A., 2001. Lumped-element technique for the measurement of complex density. J. Acoust. Soc. Am. 110, 1950. https://doi.org/10.1121/1.1401743.
Peyrega, C., Jeulin, D., 2013. Estimation of acoustic properties and of the representative volume element of random fibrous media. J. Appl. Phys. 113, 104901 https://doi.org/10.1063/1.4794501.
Pompoli, F., 2023. Acoustical characterization and modeling of sustainable posidonia fibers. Appl. Sci. 13 (7), 4562. https://doi.org/10.3390/app13074562.
Pompoli, F., Bonfiglio, A. 2020, Definition of analytical models of non-acoustical parameters for randomly-assembled symmetric and asymmetric radii distribution in parallel fiber structures, Elsevier (n.d.). https://www.sciencedirect.com/science/article/pii/S0003682X19305560 (accessed December 1, 2021).
Pompoli, F., Bonfiglio, P., Horoshenkov, K.V., Khan, A., Jaouen, L., Bécot, F.-X., Sgard, F., Asdrubali, F., D'Alessandro, F., Hübelt, J., Atalla, N., Amédin, C.K., Lauriks, W., Boeckx, L., 2017. How reproducible is the acoustical characterization of porous media? J. Acoust. Soc. Am. 141, 945. https://doi.org/10.1121/1.4976087.
Pride, S.R., Morgan, F.D., Gangi, A.F., 1993. Drag forces of porous-medium acoustics. Phys. Rev. B 47, 4964. https://doi.org/10.1103/PhysRevB.47.4964.
Rahli, O., Tadrist, L., M.M.-… de P. II, 1995, Etude expérimentale des écoulements darcéens à travers un lit de fibres rigides empilées aléatoirement: influence de la porosité, Jp2.Journaldephysique.Org 5; 1739–1756. 10.1051/jp2:1995211ï.
Ren, S., Xin, F., Lu, T., C.Z., 2017. A semi-analytical model for the influence of temperature on sound propagation in sintered metal fiber materials, Mater. Design. https://www.sciencedirect.com/science/article/pii/S0264127517308444 (accessed December 3, 2021).
Roncen, R., Fellah, Z.E.A., Simon, F., Piot, E., Fellah, M., Ogam, E., Depollier, C., 2018. Bayesian inference for the ultrasonic characterization of rigid porous materials using reflected waves by the first interface. J. Acoust. Soc. Am. 144, 210–221. https://doi.org/10.1121/1.5044423.
Rott, N. 1969. Damped and thermally driven acoustic oscillations in wide and narrow tubes, Zeitschrift Für Angewandte Mathematik Und Physik ZAMP 20:2 230–243. 10.1007/BF01595562.
Saati, F., Hoppe, K., Marburg, S., Horoshenkov, K., 2022. The accuracy of some models to predict the acoustical properties of granular media, Appl. Acoust. https://www.sciencedirect.com/science/article/pii/S0003682X21004527 (accessed December 1, 2021).
Sadouki, M., Fellah, M., Fellah, Z.E.A., Ogam, E., Sebaa, N., Mitri, F.G., Depollier, C., 2011. Measuring static thermal permeability and inertial factor of rigid porous materials (L). J. Acoust. Soc. Am. 130, 2627. https://doi.org/10.1121/1.3641402.
Sadouki, M., Fellah, Z.E.A., Berbiche, A., Fellah, M., Mitri, F.G., Ogam, E., Depollier, C., 2014. Measuring static viscous permeability of porous absorbing materials. J. Acoust. Soc. Am. 135, 3163. https://doi.org/10.1121/1.4874600.
Salissou, Y., Panneton, R., Doutres, O. 2012. Complement to standard method for measuring normal incidence sound transmission loss with three microphones, J. Acoust. Soc. Am. 131: EL216. 10.1121/1.3681016.
Salissou, Y., Panneton, R., 2007. Pressure/mass method to measure open porosity of porous solids. J. Appl. Phys. 101, 124913 https://doi.org/10.1063/1.2749486.
Smeulders, D.M.J., Eggels, R.L.G.M., van Dongen, M.E.H., 1992. Dynamic permeability: reformulation of theory and new experimental and numerical data. J. Fluid Mech. 245, 211–227. https://doi.org/10.1017/S0022112092000429.
Song, B.H., Bolton, J.S., 2000. A transfer-matrix approach for estimating the characteristic impedance and wave numbers of limp and rigid porous materials. J. Acoust. Soc. Am. 107, 1131. https://doi.org/10.1121/1.428404.
Stinson, M.R., 1991. The propagation of plane sound waves in narrow and wide circular tubes, and generalization to uniform tubes of arbitrary cross-sectional shape. J. Acoust. Soc. Am. 89, 550–558. https://doi.org/10.1121/1.400379.
Stinson, M.R., 1998. The propagation of plane sound waves in narrow and wide circular tubes, and generalization to uniform tubes of arbitrary cross-sectional shape. J. Acoust. Soc. Am. 89, 550. https://doi.org/10.1121/1.400379.
Stinson, M.R., Daigle, G.A., 1998. Electronic system for the measurement of flow resistance. J. Acoust. Soc. Am. 83, 2422. https://doi.org/10.1121/1.396321.
Suárez, L., del Mar Espinosa, M., 2020. Assessment on the use of additive manufacturing technologies for acoustic applications. Int. J. Adv. Manuf. Technol. 109, 2691–2705. https://doi.org/10.1007/S00170-020-05853-2/FIGURES/19.
Swift, G.W., 1998. Thermoacoustic engines. J. Acoust. Soc. Am. 84, 1145. https://doi.org/10.1121/1.396617.
Tamayol, A., Bahrami, M., 2009. Analytical determination of viscous permeability of fibrous porous media. Int. J. Heat Mass Transf. 52, 2407–2414. https://doi.org/10.1016/J.IJHEATMASSTRANSFER.2008.09.032.
Tamayol, A., Bahrami, M., 2010. Parallel flow through ordered fibers: An analytical approach. J. Fluids Eng., Trans. ASME 132. https://doi.org/10.1115/1.4002169/412210.
Tan Hoang, M., Perrot, C., 2012. Solid films and transports in cellular foams. J. Appl. Phys. 112, 054911 https://doi.org/10.1063/1.4751345.
Tan Hoang, M., Perrot, C., 2013. Identifying local characteristic lengths governing sound wave properties in solid foams. J. Appl. Phys. 113 https://doi.org/10.1063/1.4793492.
Tang, X., Yan, X., 2018. Airflow resistance of acoustical fibrous materials: Measurements, calculations and applications. 49; 981–1010. 10.1177/1528083718805714.
Tarnow, V., 1996. Airflow resistivity of models of fibrous acoustic materials. J. Acoust. Soc. Am. 100, 3706–3713. https://doi.org/10.1121/1.417233.

Tarnow, V., 1998. Calculation of the dynamic air flow resistivity of fiber materials. J. Acoust. Soc. Am. 102, 1680. https://doi.org/10.1121/1.420079.
Tarnow, V., 1998. Measurement of sound propagation in glass wool. J. Acoust. Soc. Am. 97, 2272. https://doi.org/10.1121/1.411952.
Tomadakis, M.M., Robertson, T.J., 2016. Viscous permeability of random fiber structures: comparison of electrical and diffusional estimates with experimental and analytical results, 39; 163–188. 10.1177/0021998305046438.
Torquato, S., 1990. Relationship between permeability and diffusion-controlled trapping constant of porous media. Phys. Rev. Lett. 64, 2644. https://doi.org/10.1103/PhysRevLett.64.2644.
Trinh, V., Langlois, V., Guilleminot, J., Perrot, C., 2019, Tuning membrane content of sound absorbing cellular foams: Fabrication, experimental evidence and multiscale numerical simulations, Mater. Design. https://www.sciencedirect.com/science/article/pii/S0264127518308293 (accessed December 1, 2021).
Tsuruha, T., Yamada, Y., Otani, M., Takano, Y., 2020. Effect of casing on sound absorption characteristics of fine spherical granular material. J. Acoust. Soc. Am. 147, 3418. https://doi.org/10.1121/10.0001210.
Umnova, O., Attenborough, K., Li, K.M., 2000. Cell model calculations of dynamic drag parameters in packings of spheres. J. Acoust. Soc. Am. 107, 3113. https://doi.org/10.1121/1.429340.
Umnova, O., Attenborough, K., Li, K.M., Umnova, O., 2001. A cell model for the acoustical properties of packings of spheres. Ingentaconnect.Com https://www.ingentaconnect.com/content/dav/aaua/2001/00000087/00000002/art00009 (accessed December 1, 2021.
Umnova, O., Attenborough, K., Shin, H.C., Cummings, A., 2005. Deduction of tortuosity and porosity from acoustic reflection and transmission measurements on thick samples of rigid-porous materials. Appl. Acoust. 66, 607–624. https://doi.org/10.1016/J.APACOUST.2004.02.005.
Umnova, O., Tsiklauri, D., Venegas, R., 2009. Effect of boundary slip on the acoustical properties of microfibrous materialsa). J. Acoust. Soc. Am. 126, 1850. https://doi.org/10.1121/1.3204087.
Utsuno, H., Tanaka, T., Fujikawa, T., Seybert, A.F., 1998. Transfer function method for measuring characteristic impedance and propagation constant of porous materials. J. Acoust. Soc. Am. 86, 637. https://doi.org/10.1121/1.398241.
Vallabh, R., Banks-Lee, P., Seyam, A.F., 2010. New approach for determining tortuosity in fibrous Porous Media. J Eng Fiber Fabr 5, 7–15. https://doi.org/10.1177/155892501000500302.
Wang, C.N., Kuo, Y.M., Chen, S.K., 2008. Effects of compression on the sound absorption of porous materials with an elastic frame. Appl. Acoust. 69, 31–39. https://doi.org/10.1016/J.APACOUST.2006.08.006.
Wilen, L.A., 1998. Measurements of thermoacoustic functions for single pores. J. Acoust. Soc. Am. 103, 1406. https://doi.org/10.1121/1.421299.
Wilen, L.A., 2001. Dynamic measurements of the thermal dissipation function of reticulated vitreous carbon. J. Acoust. Soc. Am. 109, 179. https://doi.org/10.1121/1.1333422.
Wilson, D.K., 1998. Relaxation-matched modeling of propagation through porous media, including fractal pore structure. J. Acoust. Soc. Am. 94, 1136. https://doi.org/10.1121/1.406961.
Zhou, M.Y., Sheng, P., 1989. First-principles calculations of dynamic permeability in porous media. Phys. Rev. B 39, 12027. https://doi.org/10.1103/PhysRevB.39.12027.
Zieliński, T.G., 2014. Microstructure-based calculations and experimental results for sound absorbing porous layers of randomly packed rigid spherical beads. J. Appl. Phys. 116 https://doi.org/10.1063/1.4890218.
Zieliński, T.G., 2014. Microstructure-based calculations and experimental results for sound absorbing porous layers of randomly packed rigid spherical beads. J. Appl. Phys. 116, 034905 https://doi.org/10.1063/1.4890218.
Zieliński, T.G., 2015. Normalized inverse characterization of sound absorbing rigid porous media. J. Acoust. Soc. Am. 137, 3232. https://doi.org/10.1121/1.4919806.
Zieliński, T., Venegas, R., Perrot, C., 2020, Benchmarks for microstructure-based modelling of sound absorbing rigid-frame porous media, J. Sound Vib.. https://www.sciencedirect.com/science/article/pii/S0022460X2030273X (accessed December 1, 2021).
Zwikker C., Kosten, C.W., 1949 Sound Absorbing Materials.